

Lawrence Berkeley National Laboratory

LBL Publications

Title

Surface and Catalysis Science in the Materials and Molecular Research Division

Permalink

<https://escholarship.org/uc/item/71b7g2qn>

Author

Lawrence Berkeley National Laboratory

Publication Date

1980-06-01

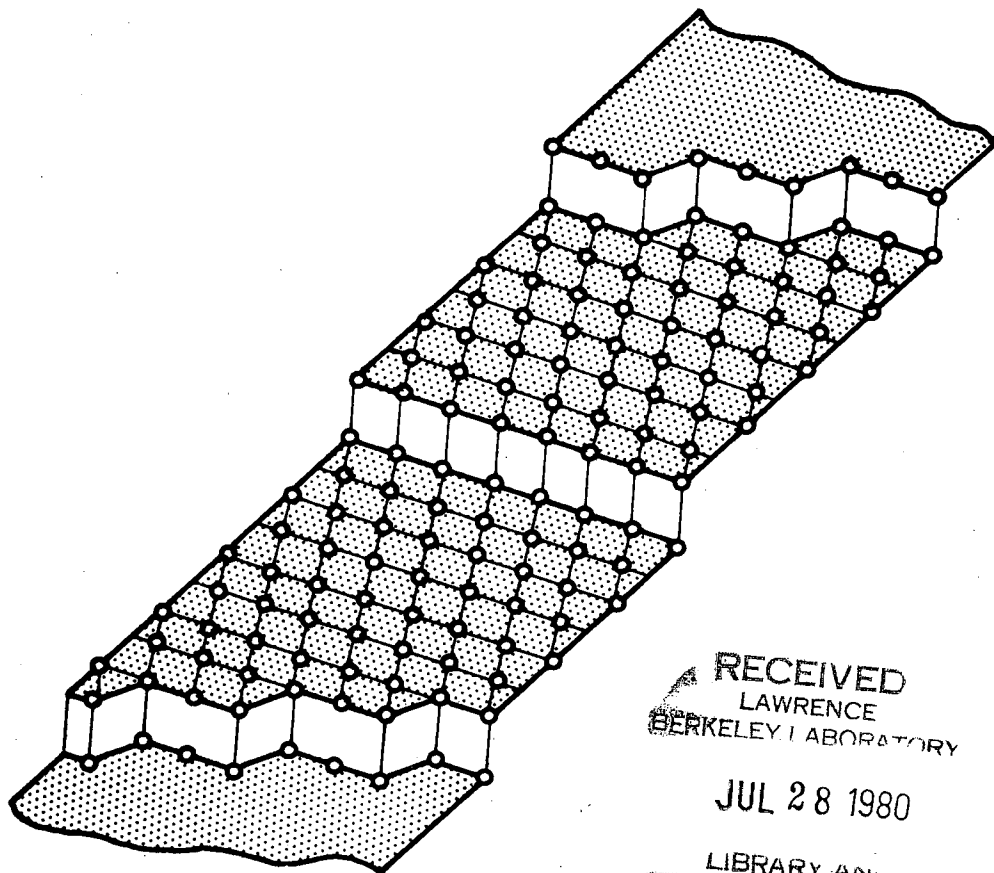
DISCLAIMER

This document was prepared as an account of work sponsored by the United States Government. While this document is believed to contain correct information, neither the United States Government nor any agency thereof, nor the Regents of the University of California, nor any of their employees, makes any warranty, express or implied, or assumes any legal responsibility for the accuracy, completeness, or usefulness of any information, apparatus, product, or process disclosed, or represents that its use would not infringe privately owned rights. Reference herein to any specific commercial product, process, or service by its trade name, trademark, manufacturer, or otherwise, does not necessarily constitute or imply its endorsement, recommendation, or favoring by the United States Government or any agency thereof, or the Regents of the University of California. The views and opinions of authors expressed herein do not necessarily state or reflect those of the United States Government or any agency thereof or the Regents of the University of California.

SURFACE AND CATALYSIS SCIENCE IN THE MATERIALS AND MOLECULAR RESEARCH DIVISION

Lawrence Berkeley Laboratory
University of California
Berkeley, California 94720

1980



RECEIVED
LAWRENCE
BERKELEY LABORATORY
JUL 28 1980
LIBRARY AND
DOCUMENTS SECTION

Pub 87 Rev. 3, c. 2

INTRODUCTION

Many useful devices of our everyday life have very large surface areas that are necessary for their proper functioning. One example is our brain, perhaps one of the most complex devices we know. Others include the integrated circuitry utilized in electronic or computer technology, biological membranes, and the catalysts employed in most chemical technologies to aid in the production of chemicals or synthetic fuels at optimum rate and selectivity.

The very high surface-to-volume ratio of most of these devices makes it essential that we concentrate on the study of surfaces if we are to understand their operation. The purpose of our research at the Lawrence Berkeley Laboratory (LBL) is to explore the various physical and chemical properties of surfaces of different materials ranging from metals to organic polymers in order to understand and control their behavior. Thus, we study the atomic and electronic structure, the chemical composition, and the reactivity of different surfaces.

Surfaces have two essential functions that give them special importance:

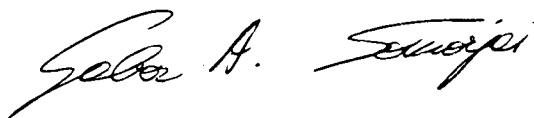
1) They are the first line of defense of a solid against hostile environments. Therefore, learning how to passivate a surface to protect

the rest of the condensed phase against chemical or mechanical deterioration is one of our goals.

2) Surfaces that are not passivated are very reactive. Unique chemical reactions take place at the solid-gas or solid-liquid interface at a high rate and specificity not occurring elsewhere. Therefore, learning how to activate a surface to optimize the desired reactivity in chemical surface reactions is another important goal.

Major areas of surface science research in the Materials and Molecular Sciences Division are the : (a) studies of the atomic and electronic structure of surfaces and adsorbates, (b) studies of the catalysis of surface reactions, and (c) investigation of the grain structure and interface structure of solids. The first two areas involve research at the solid-gas and solid-liquid interfaces and relate to the chemical and electronic properties of surfaces, while the third area investigates the properties of the solid-solid interface and relates mostly to the mechanical properties of solids.

Some specific research topics that have produced valuable surface behavior information are described by the involved principal investigators and staff scientists in the following pages.



**SURFACE AND CATALYSIS SCIENCE IN THE
MATERIALS AND MOLECULAR RESEARCH DIVISION**

CONTENTS

I. Structure of Surfaces and Adsorbed Monolayers

The Structure of Surfaces: Vibrational Spectroscopy of Adsorbed Molecules by High Resolution Electron Energy Loss Spectroscopy <i>Gabor A. Somorjai</i>	1-1
The Structure of Surfaces: Clean Metal Reconstructions <i>Gabor A. Somorjai</i>	2-1
Photoelectron Diffraction Measurements of Sulfur and Selenium Adsorbed on Ni(001) <i>David A. Shirley</i>	3-1
Raman Spectroscopy of Molecules Adsorbed on Single Crystal Metal Surfaces <i>Charles B. Harris</i>	4-1
The Electronic Structure of Physi- and Chemisorbed Molecules on Single Crystal Metal Surfaces <i>Charles B. Harris</i>	5-1
Infrared Surface Spectroscopy <i>Paul L. Richards</i>	6-1
Non-Radiative Electronic Energy Transfer from Photo-excited Molecules to Metal Surfaces <i>Charles B. Harris</i>	7-1
Electronic Excitation and Reaction Chemistry of Transition Metal Carbonyls <i>John S. Winn</i>	8-1
Chemical and Physical Properties of Small Metal Clusters and Metal-Ligand Fragments <i>John S. Winn</i>	9-1
Transition Metal Surfaces <i>Marvin L. Cohen</i>	10-1
Solute Segregation in Supersaturated Alloys <i>K. H. Westmacott</i>	11-1
Stress Generation During Oxide Film Growth <i>K. H. Westmacott</i>	12-1
Surface Properties of Binary Alloys <i>L. M. Falicov</i>	13-1
Wetting, Spreading, and Reactions in Solid/Liquid Systems <i>Joseph A. Pask</i>	14-1
X-Ray Photoelectron Spectroscopy of Metal Coordination Compounds <i>William L. Jolly</i>	15-1

II. Reduction and Oxidation of Surfaces

Early Stages of Reduction of Nickel Oxide Single Crystals: An Investigation by Transmission Electron Microscope <i>J. W. Evans</i>	16-1
Chemical Reduction of Refractory Oxides by Atomic Hydrogen <i>Donald R. Olander</i>	17-1

The Kinetics of Heterogeneous Functions of Gases and Refractory Solids by Modulated Molecular Beam Mass Spectrometry <i>Donald R. Olander</i>	18-1
Gas Solid Reaction, Reduction of Oxides <i>L. C. De Jonghe</i>	19-1
Surface Layers in Contact with Condensed Media: Observation by Ellipsometry <i>Rolf H. Muller</i>	20-1
Effects of Catalytic Reaction Mechanisms Through the Use of Dynamic Techniques <i>Alexis T. Bell</i>	21-1
Effects of Metal Dispersion on the Performance of Fischer-Tropsch Catalysts <i>Alexis T. Bell</i>	22-1
Homogeneous Catalysts in the Reduction of Carbon Monoxide to Hydrocarbons <i>K. Peter C. Vollhardt</i>	23-1
Carbon Monoxide Hydrogenation over Clear and Oxidized Rhodium Single Crystals <i>Gabor A. Somorjai</i>	24-1
 III. Catalytic Chemistry	
Photochemistry at Semiconductor Surfaces <i>Gabor A. Somorjai</i>	25-1
Coordination Chemistry of Ni and Pt Surfaces <i>E. L. Muetterties</i>	26-1
Mechanism of the Reaction Between Organotransition Metal Alkyls and Hydrides: A Model for the Aldehyde-Forming Step in the Oxo Process <i>Robert G. Bergman</i>	27-1
Catalytic Cracking of n-Hexadecane <i>Heinz Heinemann</i>	28-1
The Building of New Catalysts: The Structures and Chemical Activities of Ordered Metal Monolayers Deposited on Crystal Surfaces of Other Metals <i>Gabor A. Somorjai</i>	29-1
 IV. Structure of Interfaces and Thin Films	
Heterojunctions <i>Marvin L. Cohen</i>	30-1
Electronic Structures and Schottky Barriers <i>Marvin L. Cohen</i>	31-1
Plasma Enhanced Deposition of Magnetic Thin Films <i>Dennis W. Hess</i>	32-1
Grain Boundaries and Ionic Conduction in Sodium Beta Alumina <i>L. C. De Jonghe</i>	33-1
Grain Boundary Phases in Silicon Nitride Ceramics <i>Gareth Thomas</i>	34-1
Interfaces in Duplex Martensites (DF) Steels <i>Gareth Thomas</i>	35-1
Austenite/Martensite Interfaces <i>Gareth Thomas</i>	36-1

Atomic Structure on Grain Boundaries in Semiconductors	
<i>Gareth Thomas</i>	37-1
Structure of the Si-SiO₂ Interface	
<i>Gareth Thomas</i>	38-1
Research Staff	39-1

THE STRUCTURE OF SURFACES: VIBRATIONAL SPECTROSCOPY OF ADSORBED MOLECULES BY HIGH RESOLUTION ELECTRON ENERGY LOSS SPECTROSCOPY

Gabor A. Somorjai

High resolution electron energy loss spectroscopy (ELS) has been developed for studies of the vibrational spectra of adsorbed atoms and molecules. In this technique a collimated beam of monochromatic electrons (~ 5 eV incident energy and 8-10 MeV energy spread) is inelastically scattered from a single crystal surface and the energy distribution of the specularly reflected beam is recorded. A schematic diagram of a spectrometer used in these studies is shown in Fig. 1.

The incident electrons excite surface vibrational modes (surface phonons, adsorbate and adsorbate-substrate vibrations) and will, there-

fore, lose energy corresponding to the frequencies of the vibrations involved. Both theory and experiment have shown that this process occurs mostly via a long range dipole interaction between the incident electrons and the adsorbed gas molecules. Since only those vibrations which give rise to changing dipole moments perpendicular to the surface can be excited, ELS and infrared spectroscopy provide similar information. The advantages of high resolution electron energy loss spectroscopy are many: it has an inherently high surface sensitivity ($\sim 0.1\%$ of a monolayer for strong scatterers); it covers a large energy range (0.05-0.5 eV, or

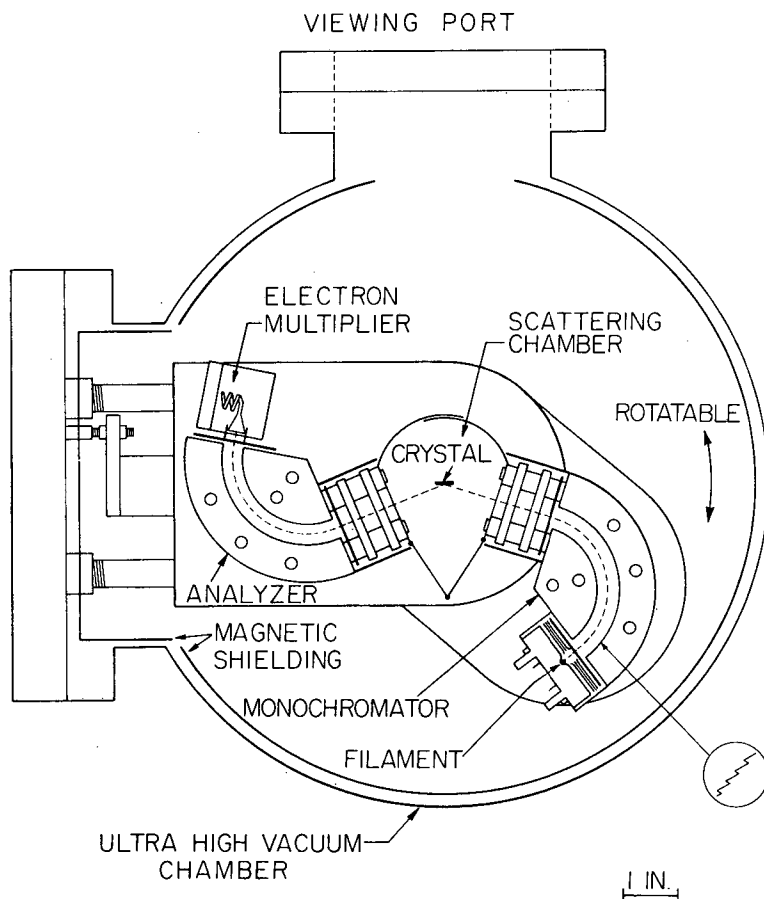


Fig. 1. Schematic diagram of a high resolution electron energy loss spectrometer.

400-4000 cm^{-1}); and it is the only technique that provides direct information about how hydrogen is bound to other atoms on surfaces.

High resolution ELS has been successfully applied to studies of the chemical bonding of numerous small molecules and hydrocarbons adsorbed on single crystal substrates. Furthermore, the bonding of reaction intermediates as a function of surface pretreatment, substrate temperature and background pressures can be readily monitored. For example, we have recently studied the molecular chemisorption and subsequent dissociation of nitric oxide on a stepped (331) orientation rhodium single crystal surface (see Fig. 2). We showed that NO which

is molecularly chemisorbed on this surface at 300 K (Fig. 2a) can dissociate into adsorbed oxygen (Fig. 2b) and gaseous dinitrogen at elevated temperatures. The vibrational spectrum obtained from the adsorption of O_2 at 300 K on this same surface is shown in Fig. 2c for comparison. By combining this data with the results from other complementary surface sensitive probes, we concluded that this surface oxygen species is an intermediate in the catalytic reduction of NO by CO over rhodium surfaces. This important reaction occurs between the exhaust gases over the catalytic converter in automobiles.

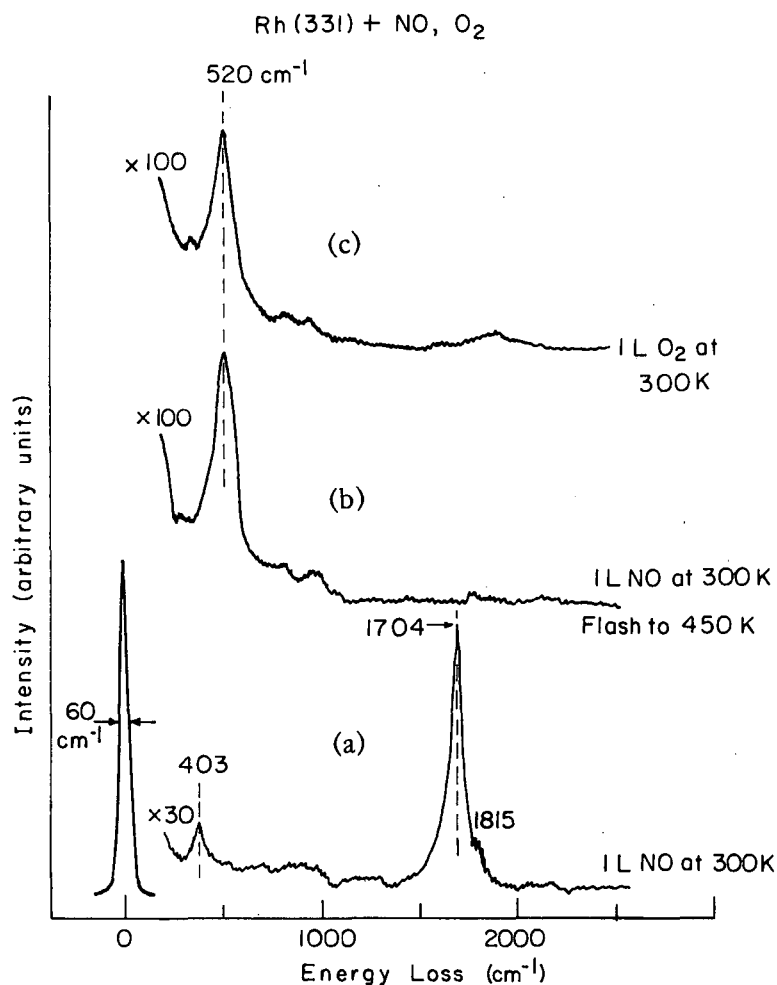


Fig. 2. (a) Vibrational spectrum showing the molecular chemisorption of NO on a Rh(331) single crystal surface at 300 K, (b) and subsequent dissociation at 450 K. (c) The chemisorption of O_2 on this surface at 300 K is shown for comparison.

THE STRUCTURE OF SURFACES: CLEAN METAL RECONSTRUCTIONS

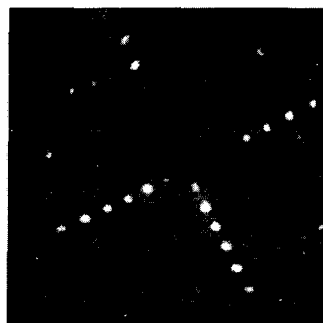
Gabor A. Somorjai

Many atomically clean metal surfaces have crystalline structures different from those expected from the known structures in the bulk of these materials. We have studied the atomic positions in such reconstructed clean surfaces [the (100) crystal faces of iridium and platinum] by means of low energy electron diffraction (LEED).

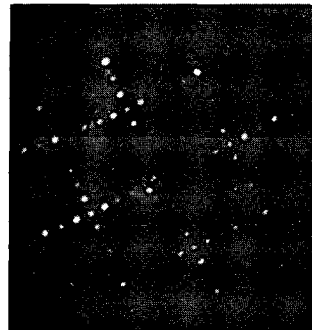
The technique of LEED has already been successfully used over the past decade to obtain

the structures of about a hundred solid surfaces. In this work its potential for handling more complex surfaces is demonstrated. The method consists of aiming a beam of monoenergetic low energy electrons (10-300 electron volts) at the ordered crystal surface which diffracts the incident electrons into a set of beams. These beams can be displayed on a fluorescent screen. Photographs of the screen are shown in Fig. 1 for the case of reconstructed Ir(100)

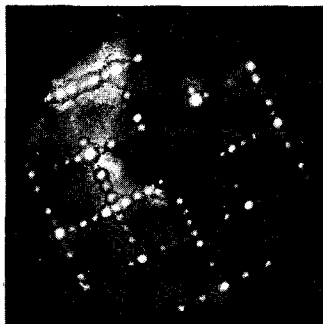
IR (100) - 5x1
 $\theta = 0, \phi = 0$
T = 300 K



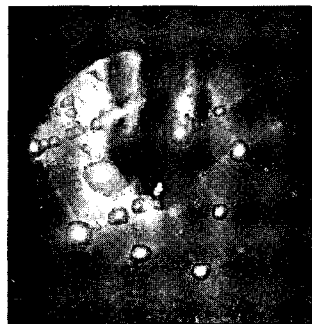
48 eV



100 eV



175 eV



273 eV

Fig. 1. LEED photographs of the reconstructed (100) crystal face of iridium at different electron energies.

surface. The intensities of the diffracted beams depend strongly on the relative positions of atoms within the topmost three or four layers of the surface. By numerically stimulating the complicated diffraction process, the atomic positions can be determined.

For the (100) crystal faces of iridium and platinum, we have been able to verify that only the topmost atomic layer rearranges and that it adopts a close-packed hexagonal structure instead of the more open square lattice structure of the bulk material, as illustrated in Fig. 2. We

have also determined that atoms in the hexagonal layer prefer the positions sketched in the left half of Fig. 2 over other positions, such as those shown in the right half of Fig. 2. Thereby the bonding mismatch between the hexagonal and square layers is more evenly distributed among the surface atoms. Furthermore, we find that the hexagonal layer is not planar but buckled so as to fit more snugly against the underlying square lattice layer. There is a small difference between the reconstructed (100) crystal faces of the Ir and Pt. The hexagonal platinum layer is

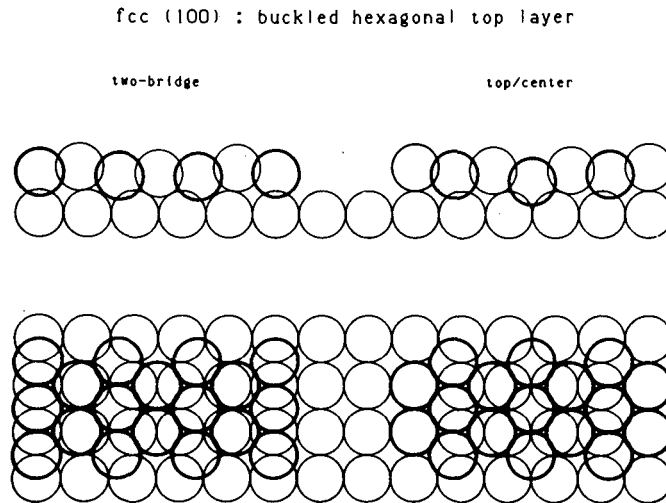


Fig. 2. Side and top views (at top and bottom, respectively) of a reconstructed (100) face of iridium surface showing at left and at right two different atomic arrangements in the reconstructed layer.

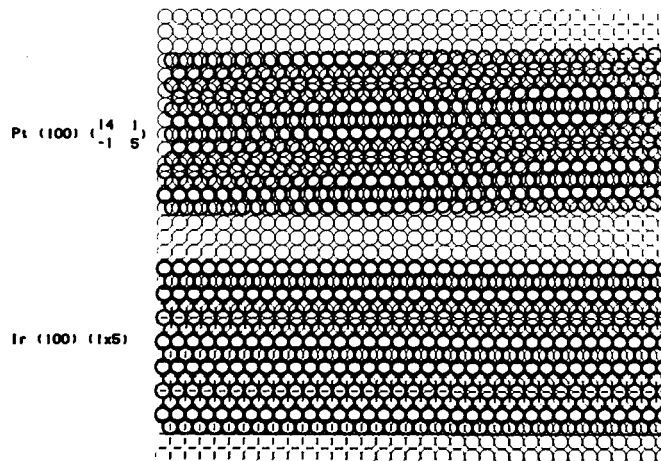


Fig. 3. Comparison of the surface structures of the reconstructed platinum and iridium crystal surfaces.

very slightly rotated (by 0.67°) with respect to the hexagonal iridium layer, as shown in Fig. 3, presenting intriguing insights into the small variations of structure that help to minimize the total surface free energy for different materials.

Another interesting aspect of our results is a bond length reduction which appears in those reconstructed surfaces. It may be that the presence of the surface induced electronic rearrangements that favor smaller interatomic distances and therefore excessively strains the

unreconstructed surface, makes the closer packed reconstruction energetically favorable.

We also use LEED to study the structure of small molecules (carbon monoxide and small hydrocarbons) bonded to metal surfaces. The structure of metallic surfaces, their behavior under changing environments, and their effect on bonded molecules are of great importance in the understanding of the chemical and physical properties of these surfaces that include heterogeneous catalysis and corrosion.

PHOTOELECTRON DIFFRACTION MEASUREMENTS OF SULFUR AND SELENIUM ADSORBED ON Ni(001)

David A. Shirley

The technique of photoelectron diffraction, which we have recently shown to be capable of determining the structure of adsorbates on metal surfaces, has been utilized to study sulfur and selenium overlayers on Ni(001). Normal photoelectron diffraction (NPD) is sensitive to adsorbate registry through d_{\perp} , the spacing between the overlayer plane of atoms and the top substrate layer. The mechanism is a two-step process—there is first an atomic-like excitation followed by scattering in the final state that introduces oscillations in the photoelectron intensity as a function of energy. These oscillations are very large and can easily be distinguished from an atomic-like cross-section.

These experiments were done on the 4° branch of Beam Line I at the Stanford Synchrotron Radiation Laboratory. The photoemission intensity of the Se(3d), Ni(3p), and Ni valence band for the p(2×2)Se overlayer on Ni(001) was measured as a function of electron kinetic energy over the range $90 \text{ eV} \leq h\nu \leq 250 \text{ eV}$. Diffraction maxima occur at different energies on each curve. Both adsorbate and substrate levels show large NPD oscillations, including multiple scattering peaks.

We have used the NPD curve for the Se(3d) core level to show that the selenium atoms of a p(2×2) Se overlayer sit in the fourfold hollow site on Ni(001) with a d_{\perp} of 1.55 Å. This result was determined from the excellent agreement between the experimental NPD curve and the curve calculated by Li and Tong for d_{\perp} of 1.55 Å, as shown in Fig. 1. Note the similarity of the peak positions of the NPD curves and the LEED (00) I-V curve, although the intensities are quite different. The system c(2×2) S-Ni(001) was also studied, and the sulfur atoms were found to sit in the fourfold hollow site, with a d_{\perp}

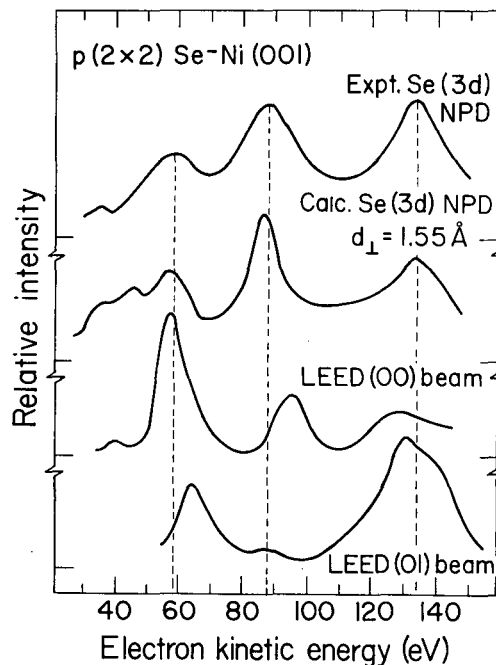


Fig. 1. NPD curve for Se(3d) electrons from p(2×2) Se-Ni(001), compared with theoretical curve by Li and Tong, and LEED-beam curves by Demuth and Rhodin.

of 1.3 Å, the same value reported from LEED and other photoemission analyses.

NPD can also be used to study disordered adsorbate systems. Disordered, low coverages of selenium on Ni(001) were found to give almost identical NPD curves as the c(2×2) overlayer. This result shows that the dominant scattering mechanism in NPD is off the substrate and not the overlayer itself; otherwise, the effect in the disordered overlayer would not be so large.

RAMAN SPECTROSCOPY OF MOLECULES ADSORBED ON SINGLE CRYSTAL METAL SURFACES

Charles B. Harris

In order to understand mechanisms of surface-mediated chemical reactions it is essential to be able to identify the chemical or molecular nature of adsorbed intermediates. It is particularly important to accomplish this for molecules adsorbed on clean single crystal surfaces of transition metals, which serve as prototype catalysts, and for which many of the modern analytical methods of surface science have been developed. Vibrational spectroscopy offers the most direct approach to the study of the structures of bound intermediates. There are currently two methods by which the vibrational spectra of molecules adsorbed on the surfaces of single crystal solids may be obtained. Infrared spectroscopy, either by reflectance, or ellipsometry, has been used to obtain spectra of strongly absorbing molecules, chiefly carbon monoxide. While the spectral resolution is quite high the sensitivity demonstrated has been rather low, and its use is not widespread. High resolution electron loss spectroscopy (HRELS), on the other hand, is characterized by rather poor resolution ($50\text{-}100\text{ cm}^{-1}$) but is extremely sensitive. It is clearly desirable to

have a method that would combine the sensitivity of HRELS with the spectral resolution obtainable by infrared absorption.

We are pursuing two approaches in parallel, each designed to effectively increase the sensitivity of Raman spectroscopy. The first program is directed towards elucidating the mechanism of the Giant Raman Effect, in which the scattering cross section for molecules adsorbed on metal surfaces (chiefly silver) apparently increases by as much as six orders of magnitude. Although observed primarily on electrode surfaces, we have begun a systematic investigation of this phenomenon on clean, well characterized single crystal surfaces, under ultrahigh vacuum. When understood, this phenomenon may be exploited to obtain Raman spectra using conventional photon counting methods.

The second approach involves the use of an optical multichannel analyzer to effectively increase sensitivity. The improvement in efficiency, due to the parallel nature of the detector, is about three orders of magnitude, making it possible to obtain spectra even in the absence of

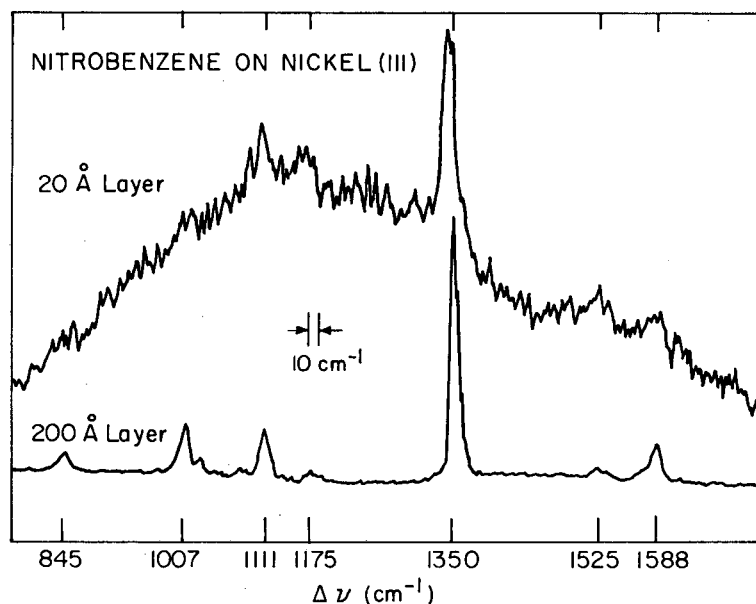


Fig. 1.

the Giant Raman Effect. The sample is contained in an ultrahigh vacuum chamber which is equipped with LEED/Auger electron optics and a quadrupole mass spectrometer to monitor the surface cleanliness and structure, and the composition of background and reactive gases. The chamber is equipped with ports to permit high efficiency optical excitation at three work stations, allow laser stimulated desorption, laser-induced structural changes, and laser-excited Raman and luminescence measurements to be carried out. Additionally the chamber is equipped with an automated scanning ellipsometer to measure the thickness of adsorbed layers as well as their complex dielectric functions from the near infrared to the near ultraviolet.

Preliminary results of our efforts to obtain ordinary, spontaneous Raman spectra of physisorbed molecules are shown in Fig. 1. The lower spectrum is for a relatively thick ($\sim 200 \text{ \AA}$) layer of nitrobenzene physisorbed on a Ni(111) surface. The spectrum obtained is of high quality and excellent (10 cm^{-1}) resolution, with all band positions corresponding closely to literature values, and the intensity ratios giving some indication of new selection rules imposed by the boundary conditions of the electromagnetic fields at the surface. The upper spectrum is for a thin layer ($\sim 20 \text{ \AA}$) which corresponds to only a few monolayers, as verified by Auger spectroscopy. The prominent features of the lower spectrum are still observed.

THE ELECTRONIC STRUCTURE OF PHYSI- AND CHEMISORBED MOLECULES ON SINGLE CRYSTAL METAL SURFACES

Charles B. Harris

It is crucial to the understanding of metal surface catalysis that one understand the changes in the electronic properties of molecules adsorbed on metal surfaces. In an effort to illuminate these interactions on clean metal surfaces, we have developed high precision spectroscopic ellipsometry to the extent that we can measure the spectra of molecules adsorbed on single crystal surfaces at submonolayer coverage. By employing suitable analytic models, we have obtained spectra of the electronic transitions for molecules such as aromatic hydrocarbons adsorbed on the Ni(111) surface.

The experiments are performed in an ultrahigh vacuum chamber of our design. The clean-

liness of the crystal, its surface regularity, and the composition of the atmosphere interacting with the crystal are monitored with modern surface analysis techniques. The composition and topography of layers deposited onto the surface can also be determined. Features of particular interest in this system are related to the difficulties in doing spectroscopy on solids within the restrictions of an ultrahigh vacuum environment.

To study both the physisorbed state and chemisorbed states of molecules on single crystal metal surfaces, the crystal can be cooled to liquid helium temperatures with a unique UHV-compatible cryostat. The sample tem-

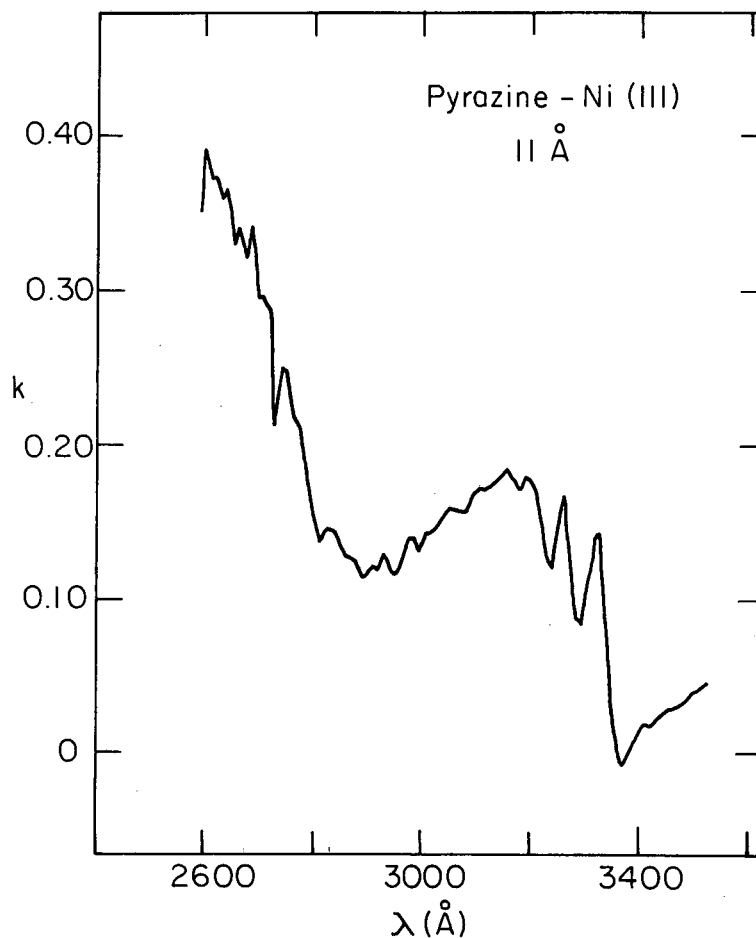


Fig. 1.

perature is continuously variable from 10 to 500 K. Finally, the entire spectroscopic apparatus is automated and under the control of a PDP 11 minicomputer. This computer is also used in the complex data analysis required to actually obtain spectra of adsorbed molecules.

Although the relatively weak interactions between physisorbed molecules and a metal surface reveal little information regarding catalytic activity, the weakly perturbed adsorbed molecules provide a cornerstone for the understanding of the more complex chemisorbed case. As an example of this, the spectra of physisorbed annealed pyrazine is shown in Fig. 1. The pyrazine spectrum shows both the ${}^1A_{1g} - {}^1B_{3u} ({}^1n\pi^*)$ and ${}^1A_{1g} - {}^1B_{2u} ({}^1\pi\pi^*)$ transitions. The vibrational progression of the ${}^1n\pi^*$ shows a small shift from the molecular crystal spectrum, indicating some influence of the metal surface. Furthermore, polarization and boundary condition restraints suggest a geometry for the pyrazine molecules with their N-N axis tipped between 30° and 45° with respect to the surface normal. Thus, even for these weakly interacting systems, the perturbing effects of the surface are revealed.

The case of a molecule chemisorbed on a metal surface is significantly more complex than the physisorbed case. The nature and strength of the many possible interactions of the molecule with the surface are not well understood. As an example of the difference which emerges during chemisorption, the spectrum of pyrazine chemisorbed on Ni(111) is given in Fig. 2. This represents the first optical spectroscopy of chemisorbed hydrocarbons on single crystal metal surfaces. For molecules adsorbed at 300 K and probed at 30-50 K, the most notable features are a broad weak band centered at approximately 3150 \AA and the shoulder of a stronger band beginning around 2700 \AA and extending below our detectable wavelength region as illustrated in Fig. 2. However, with extended annealing at 500 K, several new broad features appear in the visible region and the 2700 \AA peak disappears from the spectrum. This evidence suggests a rich chemistry for adsorbed molecules that can be exploited utilizing optical spectroscopic techniques.

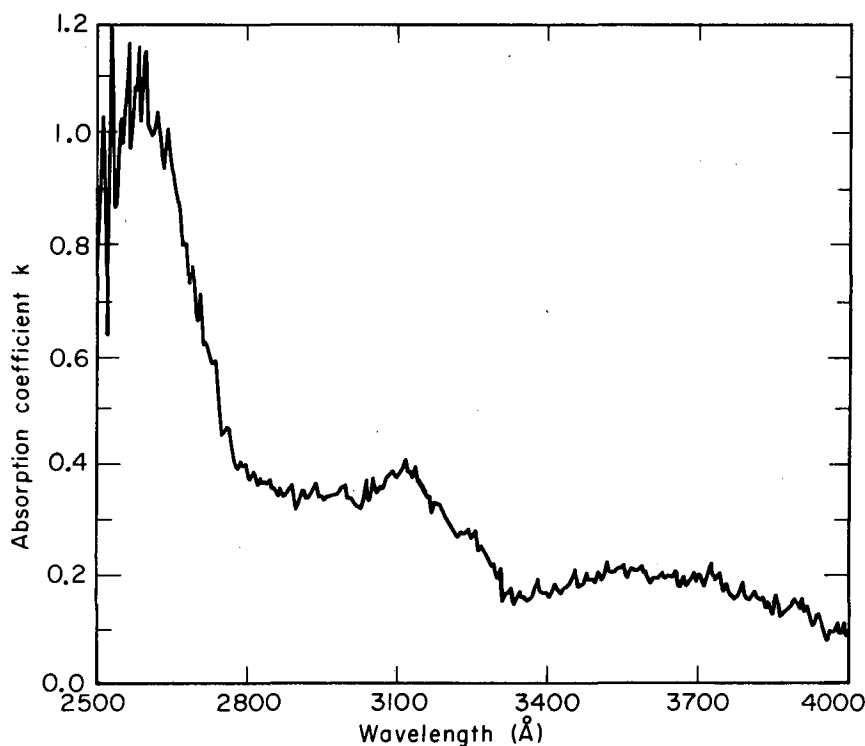


Fig. 2.

INFRARED SURFACE SPECTROSCOPY

Paul L. Richards

A novel thermal detection scheme has been developed and combined with the techniques of rapid-scan Fourier-transform infrared spectroscopy to measure surface vibrational spectra with an unsurpassed combination of sensitivity, resolution, and spectral range. Molecules adsorbed on metal surfaces are detected by attaching a doped germanium thermometer to the sample, cooling the assembly to liquid helium temperatures, and measuring the temperature changes that occur when infrared radiation is absorbed. The sample is mounted in an ultrahigh vacuum chamber in which its surface can be repeatedly cleaned, heated, exposed to gas molecules, and cooled to 1.6 K for the infrared measurements.

The vibrational spectrum of a surface can reveal a wealth of information including the identity of adsorbed molecules, the nature of their bonds to the surface, and the strength of their interactions with each other. As an example, Fig. 1 shows the absorption spectrum for different surface coverages of carbon monoxide molecules chemically adsorbed on an evaporated nickel film. The appearance of distinct absorption lines indicates that CO molecules are bonded to different lattice sites on the nickel surface. Comparison of these spectra with published data for (100) and (111) nickel surfaces suggests that the polycrystalline evaporated films consist mostly of (100) faces. We associate the changes in the relative intensity of the two strong absorption lines with transitions between different ordered phases of the CO layer, each of which is stable over a limited range of surface coverages. This interpretation is supported by the fact that the relative intensity changes do not occur when the measurement is repeated on a disordered ion bombarded nickel film.

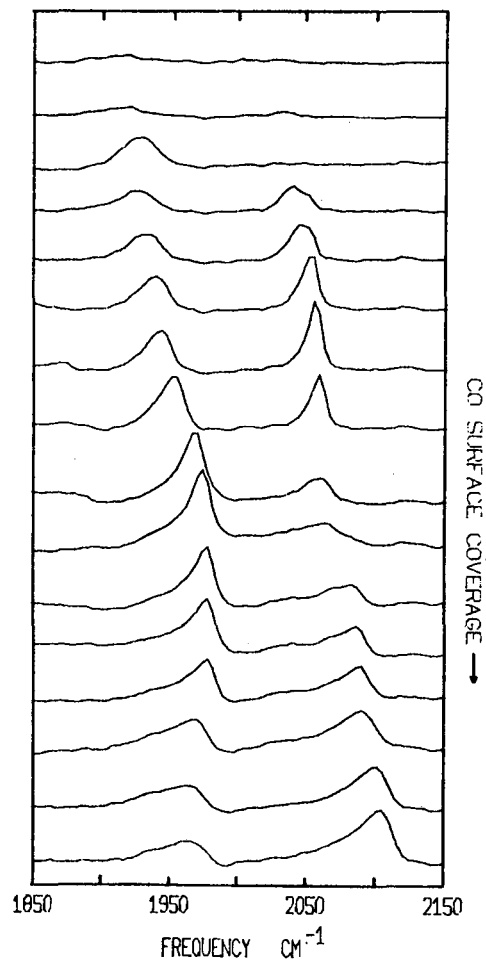


Fig. 1. Infrared spectra as a function of the surface coverage of CO molecules adsorbed on an evaporated nickel film.

NON-RADIATIVE ELECTRONIC ENERGY TRANSFER FROM PHOTO-EXCITED MOLECULES TO METAL SURFACES

Charles B. Harris

Photoassisted catalysis is potentially an exciting new area of research in surface science. In order to be able to elucidate photochemical reaction mechanisms for molecules adsorbed on surfaces it is important to understand the pathways for energy migration and relaxation introduced by the presence of the surface. The variation in fluorescence quantum yield of a dye with distance from a metal surface is reasonably well understood for distances between 50 and 5000 Å. We are interested in extending these measurements from 50 Å down to the point where the molecule is in intimate contact with the surface, either physisorbed to it. Our goal is to test the adequacy of the classical theory in this regime, which has been experimentally inaccessible thus far.

A thin layer of argon is physisorbed onto the surface of a nickel single crystal under ultrahigh vacuum at 10 K. The thickness of this layer is measured ellipsometrically. Then a thin (~ 10 Å) layer of an organic molecule is deposited onto the argon which is acting as an inert dielectric spacer. The phosphorescence intensity from the molecule is then measured as a function of the argon layer thickness. Classical image dipole theory predicts an inverse cubic dependence of the energy transfer rate upon distance in this regime. This dependence is also expected if a Forster-Dexter dipole-dipole mechanism is operative. The results of our preliminary experiment are shown in Fig. 1, with the inverse cubic dependence shown for comparison. These data are consistent with the predictions of the classical treatment down to about 50 Å. More refined experiments are necessary below 50 Å to determine the distance dependence accurately and to further assess quantum mechanical effects not contained in the classical theory model.

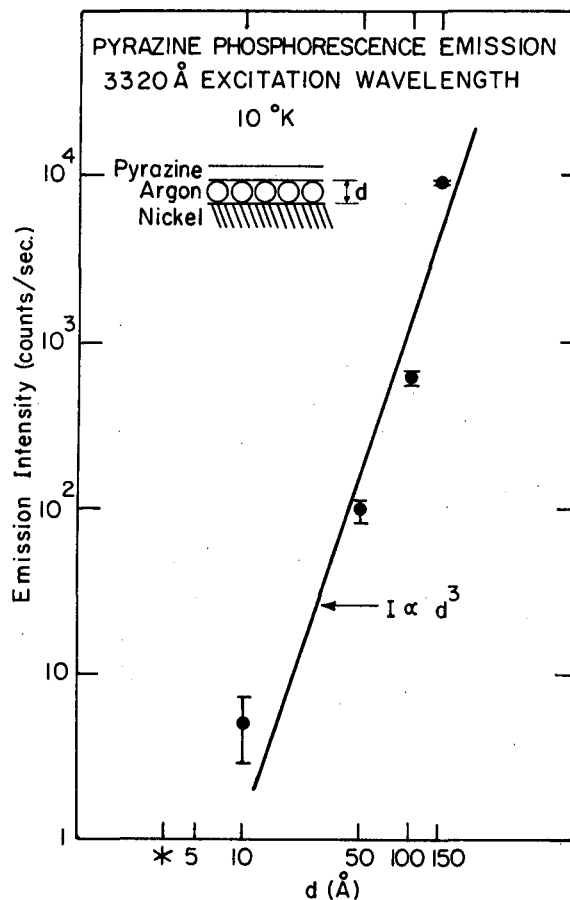


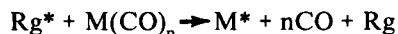
Fig. 1.

ELECTRONIC EXCITATION AND REACTION CHEMISTRY OF TRANSITION METAL CARBONYLS

John S. Winn

The analogy between the metal surface to adsorbate bond and the metal atom (or cluster) to coordinated ligand bond has long been recognized as a means of investigating surface and catalysis properties on potentially simpler model compounds. The structure and reactive properties of transition metals are not likely to be fully understood without the study of small, isolated metal carbonyls and other organometallic compounds. These compounds, especially the carbonyls, are experimentally convenient for gas phase study due to their high volatility at moderate temperatures. Moreover, we have found a new effect which permits us to strip the compounds of their coordinating ligands and to study the chemistry of gas phase transition metals at low temperatures.

The new method we have discovered is collisional electronic energy transfer from metastable rare gas atoms. In a single collision, the elementary process



was observed by monitoring the chemiluminescence intensity and spectrum. Several features of this process were investigated at length. First, it was found that the metal was produced in a series of excited states which were not spin-differentiated. Thus, among all the excited states produced are several which are either optically metastable or are characterized by exceptionally long radiative lifetimes. Since the experiment is done in a low pressure, fast flow system, distance along the flow is directly related to time. We can thereby follow subsequent reactions of metal atoms in various types of excited states which are lifetime differentiated by the flow itself.

The second feature of this process is the nature of the dissociation dynamics. We assumed that the rate of production of a given excited state of the metal was proportional to the density of states of the products. This density of states is, of course, a function of the energy available to the products (the CO ligands), and thereby a function of the energy of the excited state of the metal atom. More importantly, the density of states is a function of those degrees of freedom of the exiting CO products that are active. We have found that our data are well represented by a model in which the CO products translate in only one dimension (a radial reaction coordinate), are not allowed to rotate, and are allowed the full statistical amount of vibrational excitation. Besides being a physically satisfying model of the dissociation dynamics, this theory allows us to invert spectral intensities, via the density of states arguments, to yield metal-ligand bond energies in compounds where these values are unknown. Data on the $\text{Fe}(\text{CO})_3\text{C}_4\text{H}_6$ (iron tricarbonyl butadiene) flame have been interpreted by this model and yield an iron-butadiene binding energy of 50 ± 10 kcal/mole.

Work is continuing towards extensions of these bond energy calculations to other molecular systems as well as to the study of the reaction chemistry of ground and electronically excited Ni and Fe (monitored by both chemiluminescence and mass spectrometry) and to the extension of these methods to metal cluster compounds such as the polynuclear metal carbonyls.

CHEMICAL AND PHYSICAL PROPERTIES OF SMALL METAL CLUSTERS AND METAL-LIGAND FRAGMENTS

John S. Winn

Just as the properties of a nitrogen atom are vastly different from those of the N_2 molecule, one should expect the chemical and physical properties of, for instance, Fe_2 to be different from those of a single Fe atom. Our approach to the analysis of these differences has been to use a variety of molecular beam methods to generate metal atoms, metal clusters, and metal-ligand fragments that can be studied under isolated conditions.

There are two types of experiments that we have begun. The first uses adiabatic expansion of a metal-containing vapor to generate free metal atoms by pyrolysis of a metal carbonyl followed by condensation of the atoms in the expansion itself to yield a distribution of metal clusters (dimers, trimers, etc.). We can interpose various devices between the source and the mass spectrometer detector to analyze various physical properties of the clusters or the metal-ligand fragments that result from the expansion. One example is the use of an inhomogeneous magnetic field which deflects atoms or molecules to greater or lesser extents depending on the magnetic moment of the species, as in the classical Stern-Gerlach experiment. Moreover, if the molecular beam is sufficiently monochromatic in velocity and if the spatial resolution is sufficiently high, the deflection pattern splits into a pattern characteristic of the spin quantum states of the molecule. In this way we can distinguish the spin multiplicities of transition metal clusters or metal-ligand fragments such as FeCO.

The second type of experiment probes the reaction chemistry of metal-ligand fragments. We simply coexpand the carbonyl or other organometallic species with a potentially reactive gas, and observe the beam composition (i.e., the product distribution) in our mass spectrometer detector. These experiments are done as a function of beam source temperature (from ambient to several hundred degrees) and total source pressure (from a few Torr to several atmospheres). An example of this type of experiment is the results from the coexpansion of $Fe(CO)_5$ with H_2 . Near $100^\circ C$, thermal degradation of the carbonyl begins. At lower temperatures, no reaction is observed, but in the vicinity of $100-140^\circ C$, the mass spectrometer begins to detect CO_2 and H_2CCO (ketene). These products are believed to result from a rearrangement of a transient $Fe(CO)_4-H_2$ intermediate, which most likely involves an initial iron hydrido carbonyl prior to rearrangement to the products. Oxidation of CO to CO_2 has only been recently acknowledged to be of importance in certain catalytic reactions, and vinylidene species (H_2CC -fragments) are found as surface intermediates. Apparently both processes are at work in the formation of ketene.

Further work in this area will explore the electronic structures of fragments such as FeCO as well as the possibilities of promoting reactions such as *cis-trans* isomerization or ring cyclization.

TRANSITION METAL SURFACES

Marvin L. Cohen

Transition metal surfaces have attracted a great deal of attention because of their active catalytic properties. Experimentally, a wealth of spectroscopic data are now available for both the clean surfaces and the various chemisorbed surfaces such as low energy electron diffraction spectroscopy (LEED) and x-ray or UV photoemission spectroscopy (XPS or UPS). On the theoretical side, the surface electronic structures are difficult to calculate because of the complication of relatively localized d electrons in addition to the plane-wave-like s,p electrons. To get a realistic picture, we developed a self-consistent pseudopotential method with a mixed-basis set of plane waves and linear combinations of localized d-orbitals to account for both characteristics of the electrons. The pseudopotentials are derived from a self-consistent calculation of atomic levels and wave functions. The systems we have investigated are a Mo(001) clean surface and one with a full-monolayer adsorption of H atoms.

For the Mo(001) surface, we found a low-lying surface resonance structure at -3.3 eV

measured from Fermi surface and two surface state structures near the Fermi surface at -0.2 and -0.6 eV. They are in excellent agreement with recent photoemission spectroscopy with correct symmetry characteristics. The work function is 4.3 eV in our calculation compared to the experimentally measured value of 4.58 eV. Neither relativistic effects nor surface relaxation is needed to obtain the characteristic structure of this transition metal surface.

With a full monolayer of H atoms absorbed at bridge sites on the Mo(001) surface, the work function varies with the hydrogen-substrate interlayer distance, d . It's identical to the experimental value of 4.9 eV for $d = 0.75 \text{ \AA}$. There are two adsorbate-induced bands that lie below the substrate bulk bands. Those are hydrogen-bonding states with the substrate. The energies at the Γ pt are -7.1 eV and -5.4 eV measured from Fermi level which can be assigned to the experimental photoemission peaks at -7.0 eV and -5.3 eV. Most of the intrinsic surface states of the clean substrate survived but move to lower energies.

SOLUTE SEGREGATION IN SUPERSATURATED ALLOYS

K. H. Westmacott

Trace amounts ($\leq 0.1\%$) of certain elements can strongly affect the properties of many engineering materials because partitioning of the solute (or impurity) atoms deposits the atoms in those regions of the lattice, such as surfaces, interfaces, grain boundaries or dislocations, which can control mechanical, physical and chemical behavior. This segregation of solute atoms to surfaces or lattice defects may occur under conditions of thermal equilibrium (Gibbsian segregation) or as a result of a thermal treatment which supersaturates the lattice with solute atoms at a temperature where atom diffusion is possible.

Recent direct studies by transmission electron microscopy have shown that this latter effect, which is commonly found in substitutional alloys, occurs also in interstitial alloys, particularly those containing carbon. It is concluded from these studies that carbon present in the lattice in excess of the solubility limit becomes strongly bound to excess vacancies (due to its large atomic misfit) and that the complex migrates as an entity. Consequently, at a suitable temperature, the co-precipitation of carbon atoms and vacancies occurs in the

lattice, on dislocations, at grain boundaries, and, by inference, at free surfaces. An example of carbon platelet formation on a dislocation and its associated precipitate denuded zone in quenched and aged platinum is shown in (a) below, while precipitate-free-zones adjacent to a grain boundary in quench-aged Ta-0.5%C is illustrated in (b). These, and other results, show that carbon precipitates in the lattice and on dislocations where their associated vacancies partially retain their identity, but not on high angle grain boundaries where the vacancies are absorbed and lost.

Many other alloy systems, fcc and bcc, substitutional and interstitial, exhibit similar behavior, and it is clear that in these materials the prior thermal history has strongly influenced the distribution and effective concentration of the solute atoms. In quenching experiments, vacancy denuded zones about $1\ \mu\text{m}$ wide are observed around sinks. Therefore, in a metal with a solute or impurity concentration at the 0.01% level and negligible low temperature solubility, half a monolayer can deposit at a surface and a complete monolayer at a grain boundary by this mechanism.

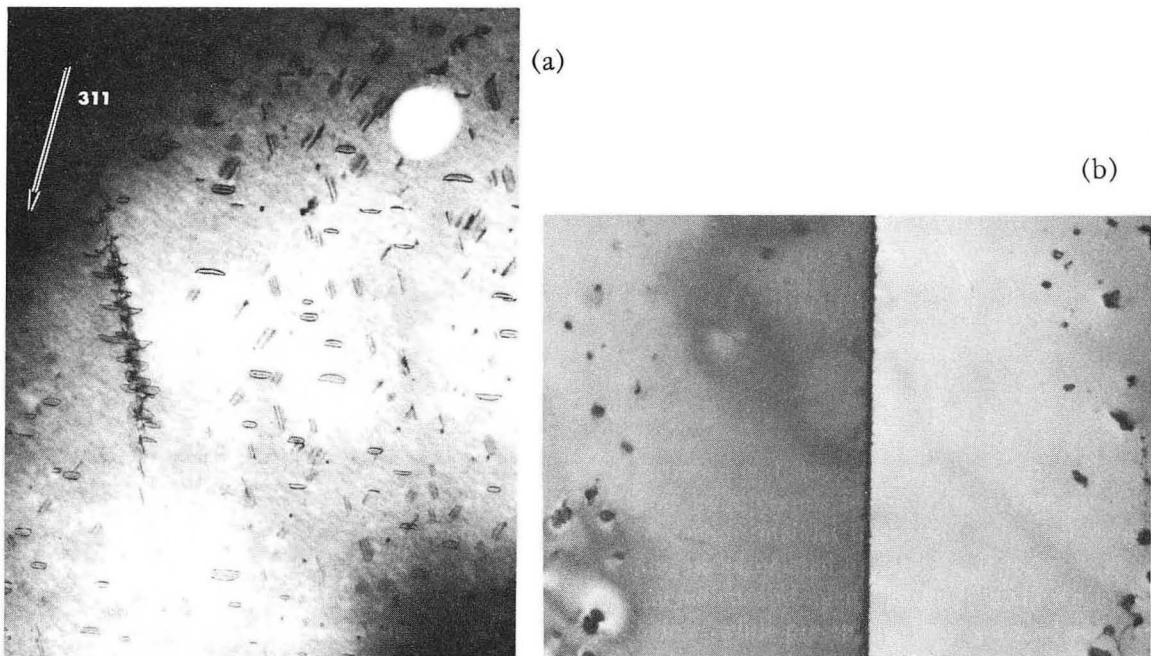


Fig. 1.

STRESS GENERATION DURING OXIDE FILM GROWTH

K. H. Westmacott

During the early stages of oxide film growth on a metal, a disparity between the lattice parameter of the oxide and the underlying metal will result in stress generation in both phases. Little is known about these stresses or how they affect the oxidation processes and rates. It has been observed, however, that the condition of the surfaces of a foil specimen electron-irradiated in a High Voltage Electron Microscope (HVEM) influences the distribution of the dislocation loops formed by the radiation. Thus, in contrast to freshly prepared samples where the loops nucleate and grow only in the center section of the foil, in foils of Al-11% Mg subjected to an ex-situ oxidation treatment prior to irradiation in the HVEM, the loops nucleate and grow rapidly at each surface near the metal-oxide interface. At an appropriate irradiation temperature the loops, which are perfect, interstitial, and all with Burgers vectors lying parallel to the foil surface, coalesce, interact, and rearrange to form irregular dislocation networks. The network geometry varies with the foil surface orientation; e.g., it is composed of a square array of pure edge dislocations in an $[001]$ orientation as shown in (a) and a roughly hexagonal network in $[103]$ foils (b). In Al-Mg alloys, the oxide that forms initially is MgO which has an appreciably larger specific volume than the underlying metal. It is therefore believed that the dislocation loops and networks form from the preferential condensation of interstitial atoms in the tensile stress field that exists near the interface.

Dynamic, in-situ experiments now in progress are designed to monitor stress build-up during the thickening of the oxide film, and also to study the role and importance of oxidation-induced vacancy injection. The magnitude of the initial stress will be varied by changing the alloy composition, and the nature of the oxide film by changing the oxidation temperature. By progressively oxidizing the foil and irradiating new areas, it may be possible to infer the underlying mechanisms through changes in the irradiation-induced microstructure.

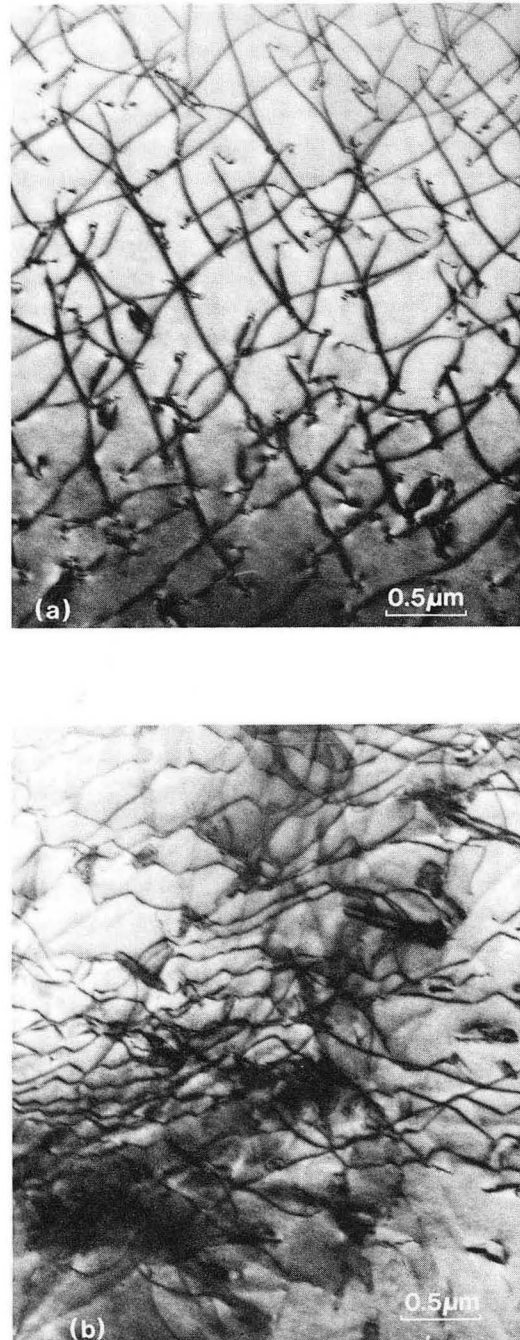


Fig. 1.

SURFACE PROPERTIES OF BINARY ALLOYS

L. M. Falicov

We have developed a theory of the equilibrium surface composition and order of crystalline binary alloys. It uses as initial information the heats of sublimation of the two component metals and the heat of formation of the alloy.

Two classes of alloys are distinguished: those that tend to form ordered binary systems, and those that tend to segregate.

For the ordering alloys it is found that the surface gets enriched in one of the components and the thickness of the enriched layer is the range of the interatomic forces. The surface enrichment and ordering are functions of the temperature. For the most common case, the surface enrichment attains its maximum value at the temperature of the bulk order-disorder transformation.

For segregating alloys the surface always gets enriched in one of the components (A). When the system separates into two phases, the phase with lower A concentration goes deep into the bulk, the phase richer in A gets close to the surface and there is a surface enriched layer which has an even higher concentration of A.

The calculation of long and short range order parameters at the surfaces has been carried out. It allows the calculation of the probability of finding given atomic cluster configurations at the surface at equilibrium.

These calculations have been applied to specific problems. For example: (1) two dimensional bimetallic clusters of $\text{Ni}_x\text{Au}_{(1-x)}$ and $\text{Ni}_x\text{Cu}_{(1-x)}$; (2) the magnetic properties of the ordering ferromagnetic alloy $\text{Fe}_{0.5}\text{Co}_{0.5}$, which for a sizeable temperature range should be more magnetic at the surface than in the bulk; (3) the possibility of an antiferromagnetic surface layer of $\text{Re}_x\text{Cr}_{(1-x)}$, an itinerant antiferromagnet.

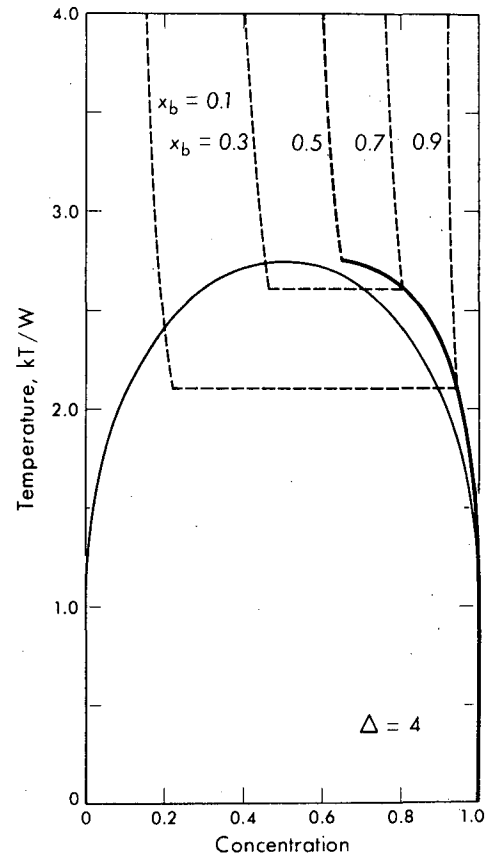


Fig. 1. Concentration-temperature phase diagram for bulk and surface in a segregating fcc alloy. The thin full line gives the concentration of the segregated phases. The thick line gives the concentration of the surface layer when segregation has occurred. The dashed lines give the concentration of the surface layer for the single-phase case and for various nominal concentrations of the bulk.

WETTING, SPREADING AND REACTIONS IN SOLID/LIQUID SYSTEMS

Joseph A. Pask

The factors that play a role in the distribution of phases, and the development of a chemical bond at interfaces, in a multiphase system are fundamental to the achievement of specific microstructures, protective coatings, and various electronic assemblies. Studies related to the thermodynamics of interfaces (solid/vapor, solid/liquid, and liquid/vapor) and reactions at interfaces that contribute to spreading of a liquid on a solid provide an understanding of such factors.

Experiments are being performed employing the sessile drop configuration under controlled ambient atmospheres and at sufficiently high temperatures for the liquid to flow and for potential reactions to occur at the interfaces. Cross-sections cut perpendicular to the interface are characterized with various analytical tools, such as an electron microprobe and scanning electron microscope, to determine the occurrence, nature, and extent of reactions.

Results from the sessile drop technique can be evaluated both from thermodynamic and mechanics viewpoints. Meaningful analyses require recognition of the occurrence of any chemical reactions. In the absence of any reaction, i.e., existence of stable or metastable equilibrium, the equilibrium sessile drop configuration is determined by the lowest interfacial energy state for the system. The existence of this state can be expressed as

$$dG = (\gamma_{sl} - \gamma_{sv})dA_{sl} + \gamma_{lv}dA_{lv} = 0 \quad (1)$$

where γ is the energy per unit area and dA is the incremental change in area. When the surface energy of the solid is larger than that of the liquid, the solid is wetted by the liquid and an acute contact angle is formed; when it is less, the solid is not wetted and an obtuse angle is formed. The equilibrium sessile drop configuration can also be expressed as a balance of the forces acting on the liquid drop due to the wetting or non-wetting of the solid by the liquid and the resisting force of the liquid generated by a configurational modification of the liquid surface area as shown in Fig. 1. This balance of forces can be expressed as

$$\gamma_{sv} - \gamma_{sl} = \gamma_{lv} \cos \theta \quad (2)$$

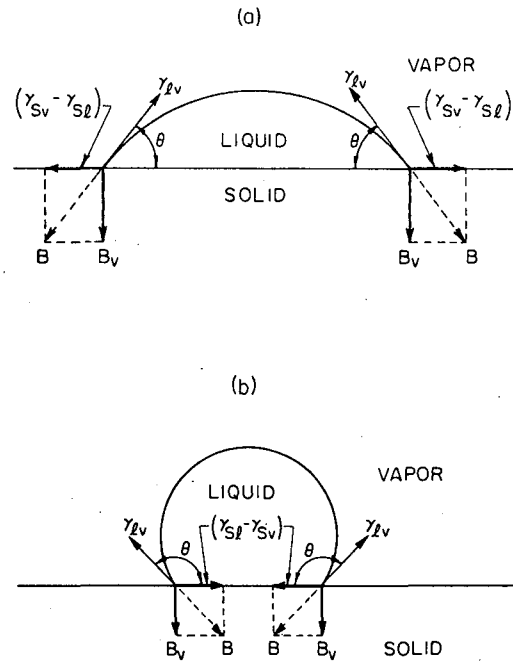


Fig. 1. Equilibrium of forces on the periphery of a sessile drop along a plane perpendicular to the interface and through the center of the drop for an (a) acute contact angle and a (b) obtuse contact angle. Force B is the resultant of the forces acting on the drop and is equal and opposite to γ_{lv} . B_v is the solid reactant force induced by the vertical component of γ_{lv} . The liquid drops are assumed to be small enough to neglect distortion by gravitational forces.

where γ in this case is tensile force and θ is the contact angle measured inside of the liquid drop. Since no release of energy occurs, no spreading occurs.

If chemical thermodynamic equilibrium does not exist and kinetics are favorable, a reaction at the interface can lead to spreading or continuing extension of the liquid surface. When the solid has a driving force for solution of a component of the liquid, the driving force for wetting plus the incremental contribution due to the free energy of the reaction can cause spreading if the

value exceeds the surface tension or energy of the liquid. This condition can be expressed at a given instant of time during the reaction as

$$\gamma_{sv} - (\gamma_{sl} + dG_R) \geq \gamma_{lv} \cos \theta \quad (3)$$

where dG_R is expressed per unit area and is a function of the rate of reaction. When the driving force for a reaction is due only to the undersaturation of the liquid relative to the solid, this solution reaction does not contribute to the driving force for wetting and spreading does not occur. After completion of the reaction and dG_R becomes zero, the system adjusts itself to a new equilibrium configuration based on the changes in all of the interfacial energies due to changes in composition caused by the reaction. The formation of a new compound at the interface causes complications.

Examples of a number of systems that are being examined on the basis of this analysis are Cu-Ag, Fe-Ag, Fe-glass, and Al_2O_3 -glass.

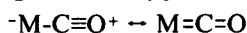
Studies of reactions have led to the theory that chemical bonding between metal and ceramic phases occurs when thermodynamic equilibrium and saturation relative to the lowest valent substrate metal oxide are realized at the interface. In the absence of such an equilibrium composition a redox reaction can occur at the interface, i.e., metal atoms of the substrate are oxidized and ions in the glass are reduced. The overall reaction thus leads to the maintenance of enrichment of substrate metal oxide in the glass at the interfacial zone. The step reactions, however, are most critical since some of them have a positive standard free energy and require controlled experimental conditions for the reaction to take place. The degree of complexity of the reactions and their kinetics is dependent upon the system. Systems being studied are Fe-glass, Co-glass, Ni-glass, alloy-glass, Ag-glass, Au-glass.

X-RAY PHOTOELECTRON SPECTROSCOPY OF METAL COORDINATION COMPOUNDS

William L. Jolly

X-ray photoelectron spectroscopy yields core electron binding energies of atoms in compounds. The binding energies are a function of chemical environment: the greater the density of valence electrons on an atom, the lower the core electron binding energy. We use this technique to study the interactions of various small molecules, such as those involved in heterogeneous catalysis, with metal atoms. We are studying the electron distribution in metal complexes that may serve as models of the metal atom-molecule interactions that occur on catalysts.

Back-bonding in a transition metal carbonyl involves a decrease in the C-O bond order of the carbon monoxide ligand and an increase in the negative charge of the oxygen atom:



In accord with this picture, we have found that, for such compounds, both the carbon 1s and oxygen 1s binding energies correlate with the C-O stretching force constants, as shown by Figs. 1 and 2. The slope of the line in Fig. 2 gives the relative average change in the oxygen and carbon binding energies on going from one carbonyl compound to another. From this we can calculate that the ratio of the negative charges transferred to the oxygen and carbon atoms in back-bonding is

$$\Delta Q_O / \Delta Q_C = 0.60$$

This is essentially the ratio of the atomic orbital contributions to the π^* orbital of a coordinated CO group. The value is qualitatively that expected for either a free CO molecule or a metal-coordinated CO molecule.

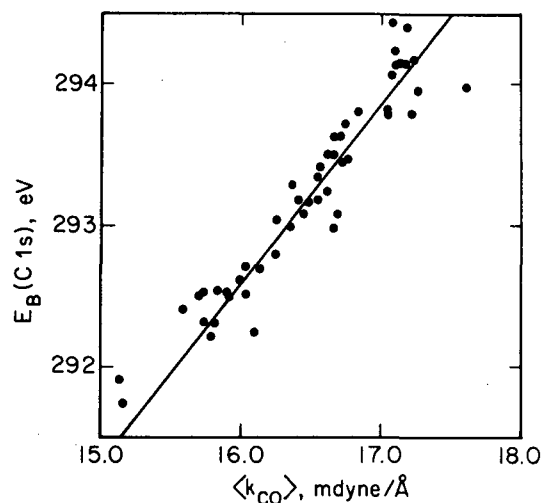


Fig. 1. Plot of carbon 1s binding energies for gas-phase metal carbonyl compounds vs C-O stretching force constants.

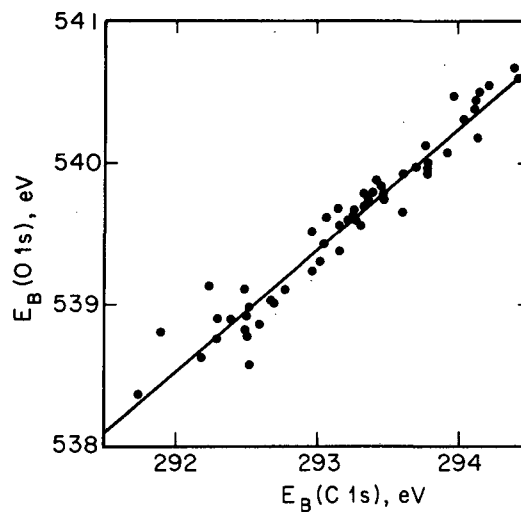
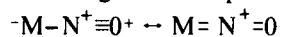


Fig. 2. Plot of oxygen 1s binding energies vs carbon 1s binding energies for gas-phase metal carbonyl compounds.

A completely analogous study has been carried out on transition metal nitrosyls, in which back-bonding is also important:



From the slope of the line in Fig. 3, we calculate that the ratio of the negative charges transferred to the oxygen and nitrogen atoms in back-bonding is

$$\Delta Q_O / \Delta Q_N = 1.08$$

This somewhat surprising result indicates that the π^* orbital of a coordinated NO^+ group is about equally distributed between the oxygen and nitrogen atoms. Apparently the effective electronegativity of the nitrogen atom in a coordinated NO^+ group is much higher than it is in free NO^+ . It is expected that studies of other transition metal complexes will give further detailed information about the nature of metal-small molecule interactions.

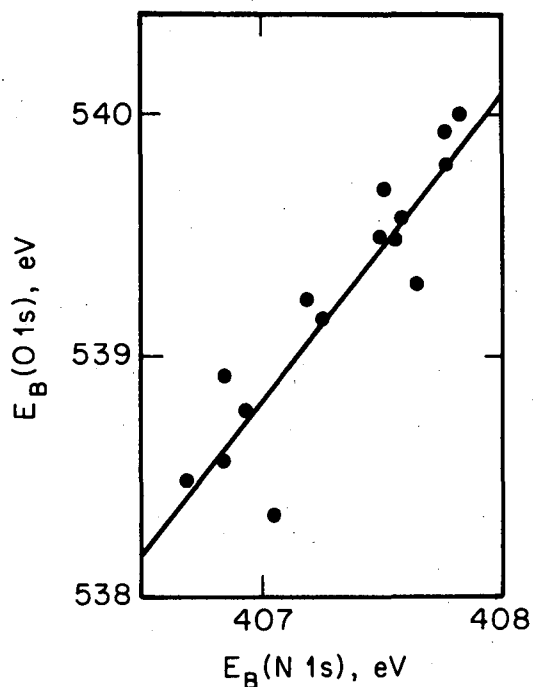


Fig. 3. Plot of oxygen 1s binding energies vs nitrogen 1s binding energies for gas-phase metal nitrosyl compounds.

EARLY STAGES OF REDUCTION OF NICKEL OXIDE SINGLE CRYSTALS: AN INVESTIGATION BY TRANSMISSION ELECTRON MICROSCOPE

J. W. Evans

Because of its practical importance, a great deal of work has been done on the reduction of metallic oxides to metals and in this laboratory the reduction of nickel oxide to nickel is being studied at all stages of reduction using a transmission electron microscope. The main emphasis of this continuing investigation is on examining these reactions *in-situ* in an environmental cell in the high voltage microscope, but great care must be taken to correlate such results with those gained by *ex-situ* reduction followed by examination in the microscope. Thus this is a brief synopsis of the results of such *ex-situ* reductions examined in a conventional 100-kV microscope.

The reductions were carried out at 200°C for times varying between 15 and 25 minutes. The reduction of nickel oxide at low temperatures occurs after an induction period where nothing appears to happen although presumably the surface is slowly losing oxygen and becoming supersaturated with respect to nickel.

Figure 1 shows a montage of bright field micrographs with their associated diffraction patterns which record the nucleation process at 15, 20 and 25 minutes.

At the earliest stage the nickel particles are seen to be in epitaxial relationship with the nickel oxide matrix and typical double diffraction reflections can be seen in the diffraction pattern. After 20 minutes the preponderance of epitaxial particles gives way to non-epitaxial nuclei as evidenced by the beginnings of powder rings in the diffraction patterns. Many of these particles can also be seen to have developed fissures and cavities at the boundaries between nickel and nickel oxide. At longer stages in the reduction, as seen in the 25-minute micrograph and diffraction pattern, agglomerations of nickel nuclei are forming, often in a banded structure, and all in a polycrystalline manner giving merely nickel powder rings in the diffraction pattern.

Thus it is observed that during the early stages of nickel oxide reduction there exist both epitaxial and non-epitaxial nickel nuclei, the latter becoming predominant as time progresses, and a plausible explanation is that non-epitaxial nuclei are formed less rapidly in the initial stages but grow more rapidly once formed.

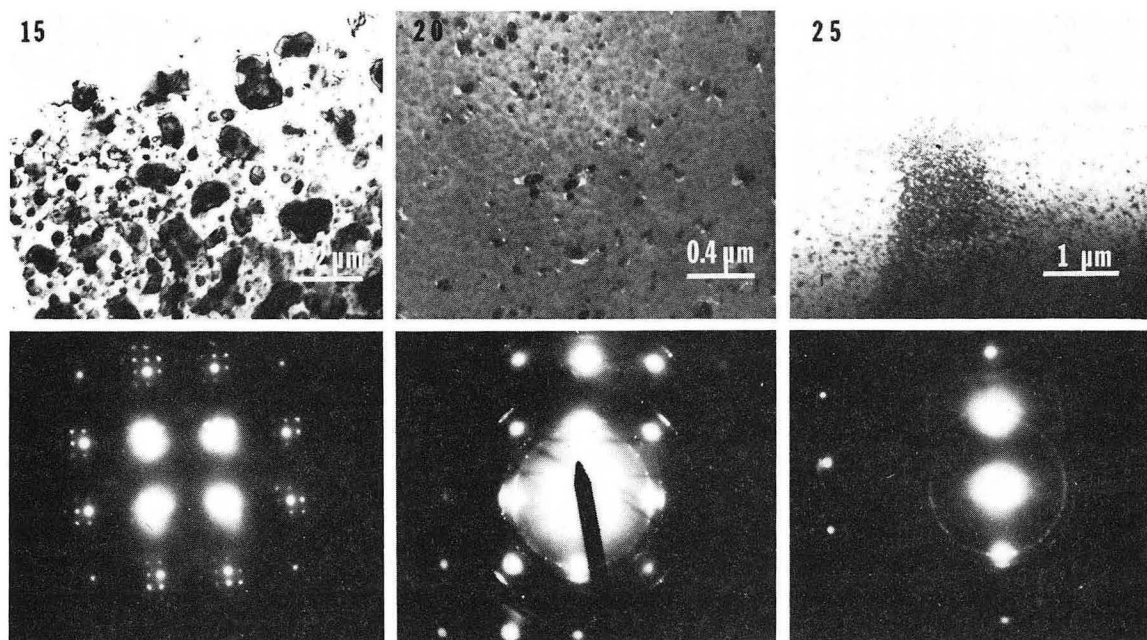


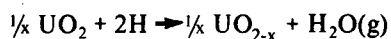
Fig. 1. Montage of bright field micrographs with their associated diffraction patterns which record the nucleation process at 15, 20 and 25 minutes.

CHEMICAL REDUCTION OF REFRACTORY OXIDES BY ATOMIC HYDROGEN

Donald R. Olander

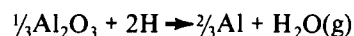
Refractory oxides are used for a number of electrically insulating components in controlled thermonuclear reactors. These components are subjected to bulk radiation damage by high-energy particles and, like graphite, may be susceptible to surface chemical attack by deuterium and tritium. The nature of the chemical attack of UO_2 and Al_2O_3 by thermal energy atomic hydrogen has been investigated by the modulated molecular beam-mass spectrometer technique. The basic difference between the two oxides is the possibility of formation of nonstoichiometric compounds. Urania contains a cation which exhibits multiple valence states and thus can form a wide range of solid solutions of the UO_{2+x} type which retain the basic fluorite structure of UO_2 . The aluminum ions in alumina, however, possess only +3 valence, so alumina is essentially a line compound with practically no deviation from the formula Al_2O_3 whether the environment is oxidizing or reducing.

Results of the UO_2/H investigation indicate that reduction of UO_2 by atomic hydrogen proceeds by the production of water vapor and hypostoichiometric urania



Contrary to UO_2 , the range of deviation from stoichiometry of $\text{Al}_2\text{O}_{3-x}$ is probably so small that even slight reduction of Al_2O_3 requires production of the metal. Because alumina

cannot be rendered hypostoichiometric, its reduction by atomic hydrogen results in production of aluminum metal



UO_2 reduction proceeds at a considerably lower temperature and with a much higher reaction probability than Al_2O_3 . The relative ease with which UO_2 is reduced by atomic hydrogen compared with Al_2O_3 is due to two factors. The first is related to the thermochemistry of the two reduction reactions. Although thermodynamics cannot be invoked to predict chemical kinetics, one can at least expect that thermochemically favored reactions should be the most readily observed.

The second feature that favors efficient reduction of UO_2 but not of Al_2O_3 is the oxygen diffusivity. As the reduction reaction proceeds at the surface, oxygen depletion of the surface layers will quickly stop the reaction unless oxygen can be transported to the surface from the bulk solid. The self-diffusion coefficient of oxygen in hypostoichiometric urania is very large compared to oxygen migration in alumina. Consequently, oxygen transport from the interior of the solid to the reacting surface takes place easily in UO_2 , but, in alumina, evaporation of the aluminum metal reaction product appears to be necessary to prevent a protective scale of Al from halting the surface reduction process.

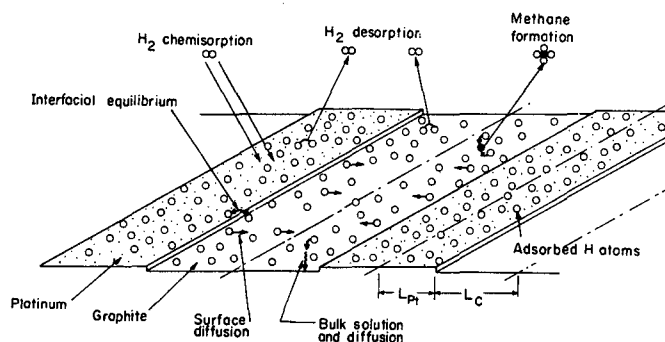


Fig. 1. Mechanism of the platinum-catalyzed gasification of graphite by molecular hydrogen.

THE KINETICS OF HETEROGENEOUS FUNCTIONS OF GASES AND REFRACTORY SOLIDS BY MODULATED MOLECULAR BEAM MASS SPECTROMETRY

Donald R. Olander

Molecular beam mass spectrometry is a powerful method for investigating the chemical kinetics of gas-solid reactions. A synchronously chopped beam of molecules or atoms impinges upon a solid surface and the consequences of the interaction are detected by an in-situ mass spectrometer which views the impingement spot. Components of the molecular beam machine shown in Fig. 1 consist of three vacuum chambers, each individually pumped,

which are interconnected by small orifices through which molecular beams pass. The molecular beam of the reactant gas is generated in the source chamber by effusion. The target chamber contains the solid reactant, and the detection chamber houses the mass spectrometer for detecting reaction products emitted from the surface.

Although catalytic reactions can be studied by this technique, our experimental program is

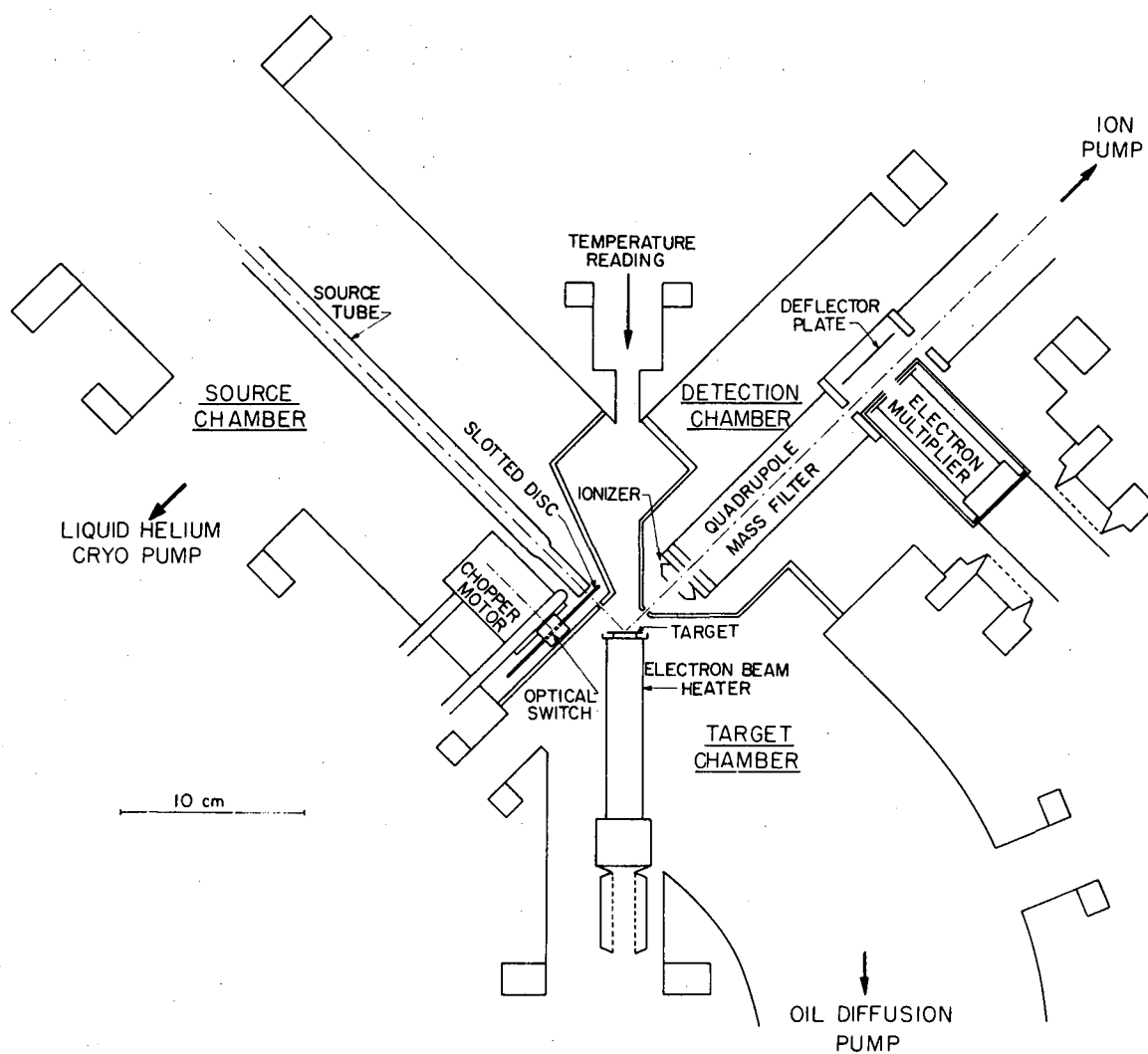


Fig. 1

devoted exclusively to corrosion-deposition reactions, wherein the solid is either: (a) consumed by the reactant gas via formation of volatile reaction products or (b) grown by cracking of the incident beam on the substrate (chemical vapor deposition). The object of the experiments is to analyze the overall heterogeneous reaction in terms of its elementary steps, which include adsorption (sticking) of the reactant, surface or bulk diffusion of surface intermediates, surface reaction of adsorbed species, and desorption of products. In addition to mechanistic interpretation of the reaction, the modulated molecular beam method permits quantitative determination of the rate constants of elementary steps involved. The power of the modulated molecular beam technique applied to gas-solid reactions is due principally to the combination of reaction probabilities and phase lag information which the experiment

provides and to the exploitation of the modulation frequency as a basic variable in addition to temperature and pressure. The reaction probability is the fraction of the incident reactant molecules that adsorb on the surface and leave as part of a product molecule. The phase lag of the product emission relative to the incident reactant flux is a measure of the mean lifetime of the beam species on the surface, and thus contains kinetic information. Conventional steady state kinetic techniques yield only the reaction probability and are not capable of as fine resolution of the reaction mechanism as is the modulated beam method.

Silicon, carbon, and silicon carbide form a set of technologically important refractory solids whose reactions with atomic hydrogen can provide insight into the chemical reactivity of these two group IV elements and their compounds.

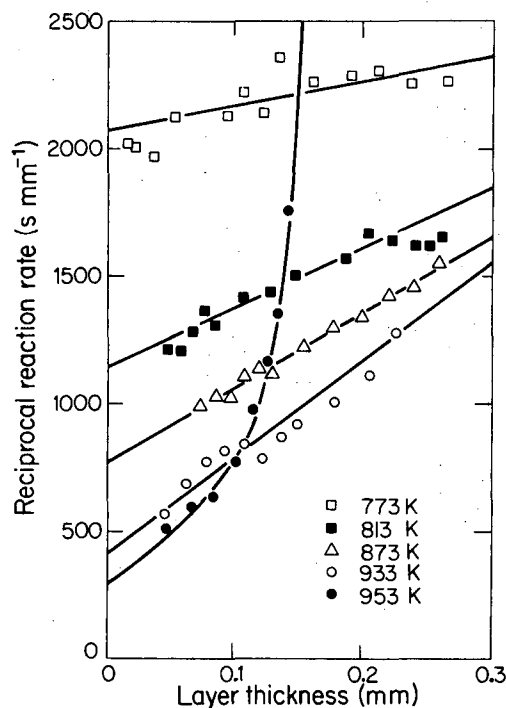
GAS SOLID REACTION, REDUCTION OF OXIDES

L. C. De Jonghe

Many problems associated with the production of energy stem from the limitations of materials performance. Chemical stability is one important material property that ultimately limits the usefulness of ceramic alloys. For oxide ceramics, rapid removal of oxygen from the lattice in a reducing environment at high temperatures is an example of an important chemical materials limitation. Ideally, the resistance of oxides to gaseous reduction might be improved by the addition of an appropriate alloying element, as is common in the protection of metals against oxidation. In reduction the product layer is porous and does not generally provide an effective barrier against further reduction. Reduction reactions can therefore proceed quite rapidly, compared to oxidation reactions, so that non-equilibrium effects at interfaces may be significant. No general analysis can cover the entire range of reduction reactions from low temperatures to high temperatures. At low temperatures catalytic effects dominate. At high temperatures, rapid structural changes in the scales may be important. However, in some intermediate temperature range, a very simplified reaction analysis is possible giving important insight into the reaction mechanisms. In this domain, modeling is often done in terms of reaction resistances comprised of three main categories: (1) The mass transfer resistance to flow of gas from the bulk stream; (2) The gas transport resistance to gas phase diffusion through the porous product layer; and (3) The interface reaction resistance. For each of these steps, rate parameters could be determined, and the dependence of these parameters on the reaction conditions can be examined. Such examination can reveal the physical significance of the various kinetic parameters. For example, the two components of the gas diffusion could be found from the pressure dependence of the effective gaseous diffusion coefficient. The interface reaction itself is also described by means of a single kinetic parameter in these models, but may actually involve a complicated set of surface reactions including adsorption,

desorption, association and so on, as well as solid state diffusion near or in the interface. Additional information such as the micromorphology of the interface reaction, besides the pressure and temperature dependence of the reaction coefficients, can shed further light on the nature of the interface reaction.

In this study, we have examined the aspects of hydrogen reduction of cobalt ferrite in the temperature range between 500°C and 800°C. We have used thermogravimetric analysis and electron microscopy to elucidate the nature of the various reaction steps in the reduction. It



1. Reduction kinetics at 100 torr for specimens reduced between 500 and 680°C. The reciprocal interface advance rate is plotted against the layer thickness calculated from the weight loss data. Note that at 600°C the kinetics no longer follow the simple relationship expressed in Eq. (1).

was found that in a temperature range between 500 and 650°C and under the reaction conditions used, the reduction reaction could be simply expressed as:

$$\dot{\xi} = \frac{P_{H_2}^{pb}}{RTc_0} \left(\frac{1}{k_r} + \frac{\xi}{D_{eff}} \right)^{-1} \quad (1)$$

Where ξ = the rate of layer thickening, k_r = interface reaction rate coefficient, D_{eff} = the effective gaseous diffusion coefficient in the porous product scale, and $P_{H_2}^{pb}$ = bulk pressure of hydrogen in the gas stream.

The mass transfer from the gas bulk to the sample appeared to be a negligible resistance. From Equation 1, it can be seen that if the inverse rate is plotted vs the layer thickness, a linear relationship should be obtained. Figure 1 shows how well the linear relationship is indeed obtained in the temperature range mentioned. However, serious deviations are observed around 680°C. The strong deviation from the simple expression for the reduction rate, Eq. (1), is due to the appearance of the reaction rate anomaly as is evident from Fig. 2. Of special interest is the behavior at 700°C where we observe an initially fast reaction rate that after some layer thickness changes to a slow reaction rate. Transmission electron microscopy has shown that the initial reaction is one where spinel is directly converted to metal. At longer times, a wustite subscale appears which is associated with the slowdown of the reaction rate. The reaction rate anomaly, and the absence of wustite in the early stage of the reaction is considered to be a kinetic effect. Indeed, the rate of growth of a small cobalt-wustite precipitate at the metal/spinel interface has to be compared to the rate of interface advance, ξ , Eq. (1). If the particle is consumed by the advance interface more rapidly than it can grow, then a continuous wustite layer cannot form. The growth rate of the wustite precipitate, v_w , at the advancing metal/spinel interface can be considered to be a first approximation to a constant for a constant temperature and pressure. From a comparison at ξ and v_w a critical layer thickness, ξ_c , can be found at which wustite can first appear. We find this critical layer thickness to be of the form:

$$\xi_c = \frac{D_{eff} P_{H_2}^{pb}}{RT} \times \left[(c_0 A^* \Delta\mu \exp(-Q_w/RT))^{-1} - RT/k_r P_{H_2}^{pb} \right] \quad (2)$$

where c_0, A^* = constants, $\Delta\mu$ = chemical potential difference determining v_w , and Q_w = activation energy for v_w . Also, there should be a temperature T_0 at which wustite is initiated immediately at the beginning of the reaction. This temperature would be one where the rate of growth of the wustite precipitate always exceeds that of the rate of spinel metal interface advance. T_0 is found to be of the form:

$$T_0 = - \frac{Q_w}{R \ln(k_3/C_0 \Delta\mu A^*)}$$

where k_3 = an interface transport coefficient.

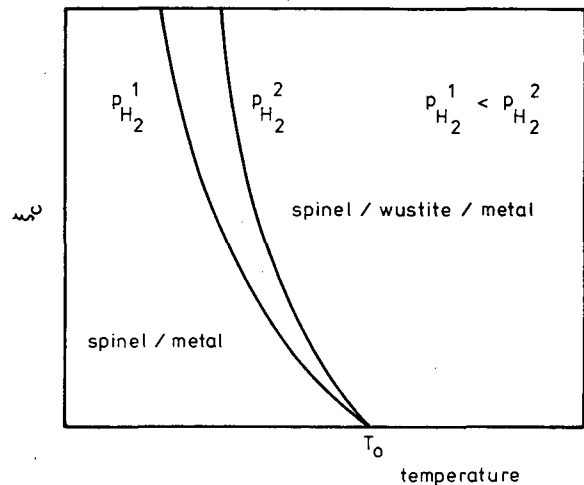


Fig. 2. Qualitative behavior of ξ_c as a function of temperature, according to Eq. (2).

Since all the kinetic parameters are not yet known, only the qualitative behavior of ξ can be considered, Fig. 2. It is apparent from this figure that the reduction rate will be characteristic of a direct spinel/metal reaction until $\xi = \xi_c$. At that point the reaction rate should become characteristic of the spinel/wustite reaction. The pressure dependence of this critical thickness should be such that at fixed temperature ξ_c it would increase with increasing bulk hydrogen pressure, and at fixed pressure ξ_c would decrease with increasing temperature. This behavior is in fact confirmed in Figs. 3 and 4 in which the layer thickness as a function of time and temperature is shown at a constant pressure (Fig. 3) and in which layer thickness is a function of time and pressure at a constant temperature (Fig. 4). A number of conclusions could be drawn from the present work:

(1) Below 660°C, the reduction of cobalt ferrite by hydrogen at reduced pressures was shown to be under mixed control of the chemical reaction at the scale/cobalt ferrite interface and of the gaseous diffusion through the scale. The importance of the gaseous diffusion resistance through the scale increases with increasing temperature. (2) The effective diffusion coefficients of gas through the scales were determined to have both Knudsen and molecular components. The changes in the diffusion coefficient as a function of the reducing conditions could be attributed to changes in the scale morphology. (3) The interface reaction was found to follow Langmuir-Hinshelwood kinetics. (4) The reaction rate minimum which was

observed at 700°C was caused by the development of a continuous subscale of cobalt-wustite. The incubation period for the development of the subscale could be attributed to the different velocities of the spinel/metal interface and of the wustite/spinel interface. A critical layer thickness was defined as a thickness of the metal scale at the moment when the subscale became continuous. The temperature and pressure dependence of the critical layer thickness was found to be in agreement with the proposed model.

Our further work will examine the nature of the interface reaction in more detail, and will clarify the role of ceramic alloying additions on the chemical reactivity towards gases.

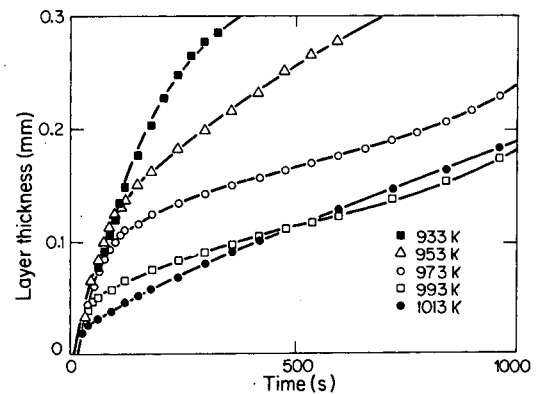


Fig. 3. Reduction kinetics at 100 torr for specimens reduced between 660°C and 740°C. Note that the switchover in kinetics occurs at smaller product layer thicknesses with increase in temperature.

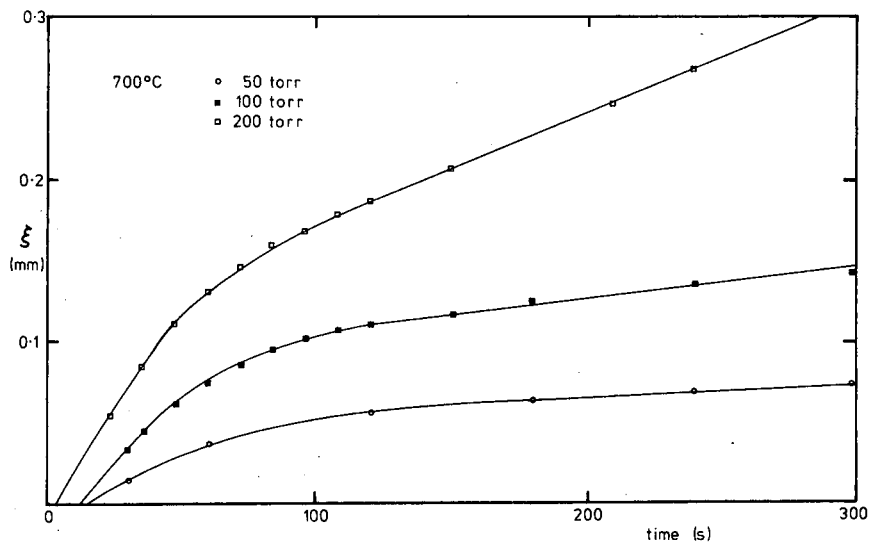


Fig. 4. Reduction kinetics at 700°C for specimens reduced between 50 torr and 200 torr. Note that the switchover in reduction occurs at smaller product layer thicknesses with decreasing gas pressure.

SURFACE LAYERS IN CONTACT WITH CONDENSED MEDIA: OBSERVATION BY ELLIPSOMETRY

Rolf H. Muller

Analysis of the elliptic state of polarization that results from the reflection of polarized light (ellipsometry) provides an extremely sensitive measure for the observation of surface layers that may be contained in any optically transparent medium. Surface coverages from less than 1% of monomolecular coverage to micrometer thickness can be determined.

A unique automatic ellipsometer that is capable of following film growth at rates up to a few micrometers per second has been built in this laboratory and is being used to elucidate electrochemical processes at metal-electrolyte interfaces.

A recurring problem in the interpretation of ellipsometer data is that a single measurement is usually subject to multiple interpretations. Although the freedom of interpretation can be

reduced if series of measurements are considered, it is often found that assumptions necessary for one segment of the measurements contradict those for another segment.

An automated computer interpretation of ellipsometer measurements of anodic film growth has now been introduced. This interpretation makes fuller use of experimental information by taking the time-dependence of the measured optical and electrical parameters into account. A continuous mass-and-charge balance is applied to a theoretical model of film formation. This model considers the simultaneous or sequential formation of several surface layers with time-varying properties via a dissolution-precipitation mechanism. The time sequence of events according to a six-layer model is illustrated in Fig. 1.

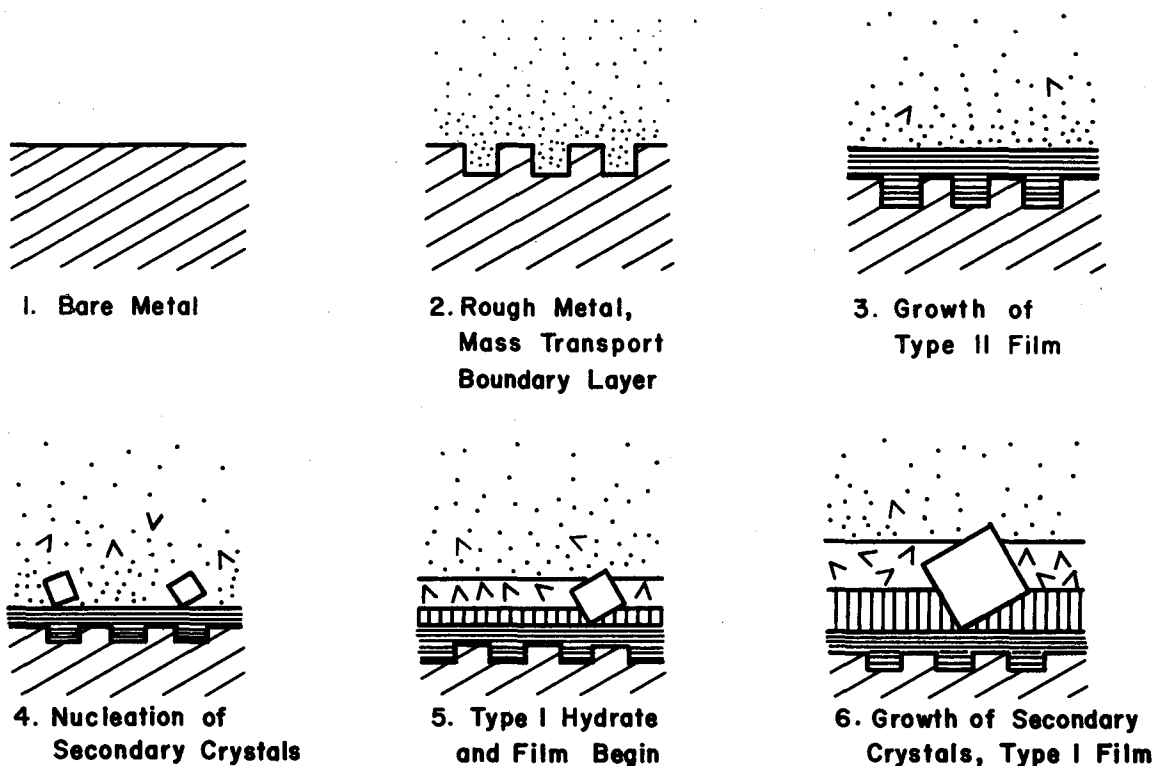


Fig. 1. Time-sequence of events in anodic film formation.

The interpretation of experimental data is accomplished by finding values for up to seven physically meaningful parameters of the film formation model that most closely reproduce the ellipsometer measurements. The fitting routine in seven-dimensional space involves a variation of all parameters until a minimum mean square deviation between measured and predicted ellipsometer measurements is accomplished. Parabolic error estimates are used to provide measures of uncertainty for the parameters thus derived. In order to search for multiple roots, a Monte Carlo routine is used in which new initial values for the minimization iteration are chosen at random.

Figure 2 illustrates the agreement between experimental measurement and model prediction that can be obtained by the interpretation procedure, which does not rely on ad-hoc assumptions and covers a large range of film growth.

Parameters of the film-formation model that can be derived from the measurements include quantities that are not directly measurable by ellipsometry, such as kinetic and transport parameters. Independent experimental evidence for the key features of the model is being obtained by the combination of ellipsometry with ion etching and Auger spectroscopy.

Ellipsometry has also been established as a new technique for the observation of mass-transport boundary layers. Simplifications in optical theory have been found and their

validity has been demonstrated with determinations of the interfacial concentration of reactants in the absence of convection, laminar and turbulent flow. Similarly, the accumulation of supporting electrolyte at an electrode surface has been determined at limiting current. The installation of digital data acquisition and rapid spectral scanning capabilities will provide new information and allow its efficient use for the *in-situ* identification of surface compounds.

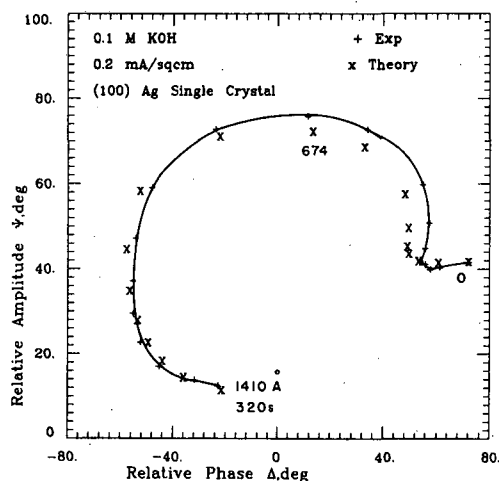


Fig. 2. Interpretation of ellipsometer measurements. Anodic oxidation of Ag(100) in 0.1 M KOH at 0.2 mA/cm². Comparison of experiment (+) and model prediction (x). Primary layer thickness (Type I and Type II films) indicated along the curve.

EFFECTS OF CATALYTIC REACTION MECHANISMS THROUGH THE USE OF DYNAMIC TECHNIQUES

Alexis T. Bell

Discrimination between mechanisms proposed to describe the progress of a chemical reaction on a catalyst surface is usually not possible using steady-state kinetic data alone. Much more sensitive tests of mechanistic alternatives can be obtained, though, from dynamic studies in which observations are made of the transient response of the catalyst and reaction system to a well-defined stimulus. In the present research, dynamic techniques are being used to study the reduction of NO by H₂ over group VIII metals.

Figure 1 illustrates the apparatus used. A self-supporting disc of the catalyst (50 mg) is contained in a small reactor which also serves as an infrared cell. Gas is fed to the reactor from one of two manifolds. By rapid switching from one to the other manifold a step function change in gas composition can be produced within 0.1 sec. The products from the reactor are continuously analyzed by a quadrupole mass spectrometer connected to a data acquisition system. Infrared spectra of species adsorbed

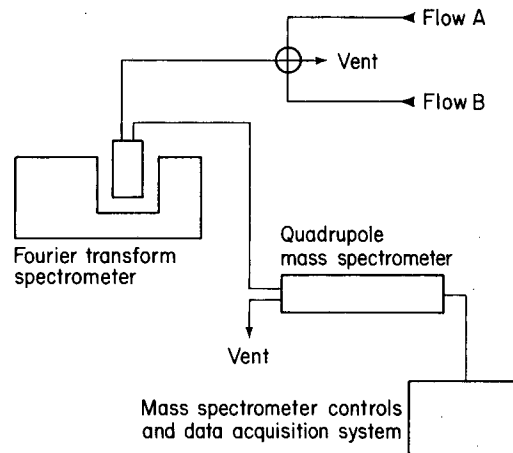


Fig. 1. Schematic of experimental apparatus.

on the catalyst surface are recorded by a Fourier transform spectrometer at a rate of 0.1 to 1.0 spectra per second. By this means, dynamic processes with time constants on the order of 0.1 sec can readily be followed through changes

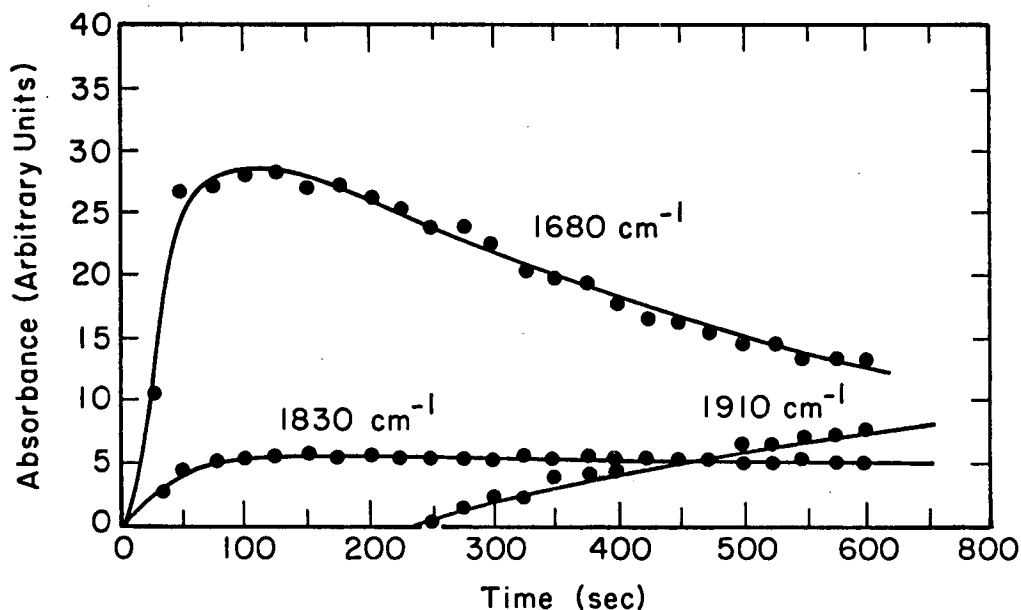


Fig. 2. Time evaluation of infrared absorption bands of NO adsorption on Rh.

in product composition and the composition of surface species. By heating the reactor at a constant rate, temperature programmed desorption and reaction spectra can be obtained.

Figure 2 shows the time evolution of different infrared bands associated with adsorbed NO when a 4% Rh/SiO₂ catalyst maintained at 150°C is exposed to a stream containing 3% NO in argon. The band at 1680 cm⁻¹ assigned to nitric oxide chemisorbed on reduced Rh as NO^{δ-} rises very rapidly and saturates in about 100 sec. Beyond this time the band intensity declines as the band at 1910 cm⁻¹ appears. This latter band is due to nitric oxide chemisorbed as NO^{δ+} and is characteristic of adsorption on an oxidized Rh surface. The remaining band at 1830 cm⁻¹ is due to nitric oxide adsorbed in a neutral state and is insensitive to the state of surface oxidation.

An example of the time evolution of products produced under dynamic conditions is illustrated in Fig. 3. The reduced catalyst is first exposed to a 3% NO/Ar stream for 15 sec and then switched over to a 30% H₂/Ar stream. Both N₂ and N₂O appear about 1.0 sec after the switch to the H₂ flow, but the formation of NH₃ and H₂O is delayed by 1.5 sec. Infrared spectra taken during the experiment show that all adsorbed NO is removed from the surface in about 4 sec. Similar experiments carried out under a variety of reaction conditions reveal that the relative intensities of the product peaks and the times at which they reach a maximum are sensitive functions of the initial NO coverage, the H₂ partial pressure during reduction, and the catalyst temperature.

Transient response data, together with the results of temperature programmed desorption and reaction experiments lead to the conclusion that NO adsorption is very rapid but that dissociation to form N and O atoms is a slow, activated process. By contrast, reactions to form N₂ and N₂O are very rapid. The reactions to form NH₃ and H₂O are slower than those to form N₂ and N₂O and are controlled by the availability of atomic hydrogen on the catalyst surface. Models of the reaction kinetics, incorporating these observations, have been developed and are now being tested. Initial results have shown that the transient response data provide a very sensitive data base for distinguishing between alternative reaction mechanisms.

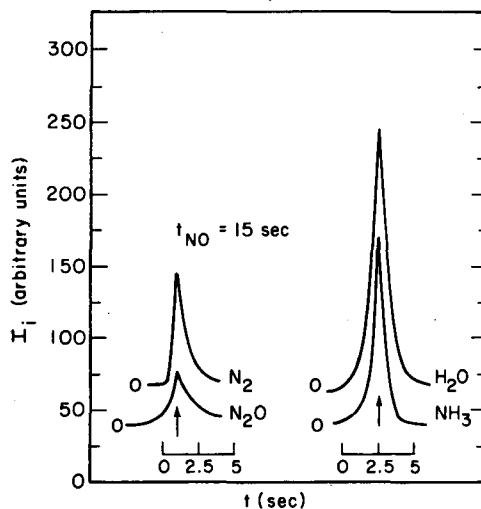


Fig. 3. Transient responses for N₂, N₂O, NH₃, and H₂O during reduction of preadsorbed NO.

EFFECTS OF METAL DISPERSION ON THE PERFORMANCE OF FISCHER-TROPSCH CATALYSTS

Alexis T. Bell

It is well recognized that the catalytic performance of supported metal catalysts can be influenced by the extent of metal dispersion and the degree of interaction between the metal and the support. The effects of these factors on the activity and selectivity of ruthenium catalysts used for Fischer-Tropsch synthesis are being investigated in this project.

High dispersion catalysts are prepared by adsorbing $\text{Ru}_3(\text{CO})_{12}$, $\alpha\text{-H}_4\text{Ru}_4(\text{CO})_{12}$ and $\text{Ru}_6\text{C}(\text{CO})_{17}$ on $\gamma\text{-Al}_2\text{O}_3$. The extent of $\text{Ru}_3(\text{CO})_{12}$ adsorption on $\gamma\text{-Al}_2\text{O}_3$ is found to depend strongly on the temperature at which the support has been dehydroxylated. Infrared spectra of alumina-supported $\text{Ru}_3(\text{CO})_{12}$ suggest that the cluster is adsorbed as a result of interactions between the carbonyl ligands with hydroxyl groups and Lewis acid sites present on the support surface. Similar interactions are proposed for alumina-supported $\alpha\text{-H}_4\text{Ru}_4(\text{CO})_{12}$ and $\text{Ru}_6\text{C}(\text{CO})_{12}$.

As shown in Fig. 1, decomposition of the supported clusters produces three surface structures, independent of the original cluster composition. The first structure is characterized by infrared bands at 2045-2050 and 1965-1970 cm^{-1} and is represented by $[\text{Ru}(\text{CO})_2\text{X}_2]_n$. The second and third structures are characterized by bands at 2130-2140, 2060-2070, and 1990-2000 cm^{-1} and are represented by $[\text{Ru}(\text{CO})_3\text{X}_2]_n$ and $[\text{Ru}(\text{CO})_4\text{X}_2]_n$, respectively. In each of the three structures X represents an oxygen atom of the alumina lattice. The nuclearity of the surface structures, n, cannot be defined from the present studies, since it is not known whether the metal lattice of the original cluster decomposes upon adsorption on the support or whether agglomeration of clusters occurs.

Complete decarbonylation of the Ru surface structures induces a stronger Ru-support interaction, which may lead to the entry of Ru ions into the support lattice and the formation of

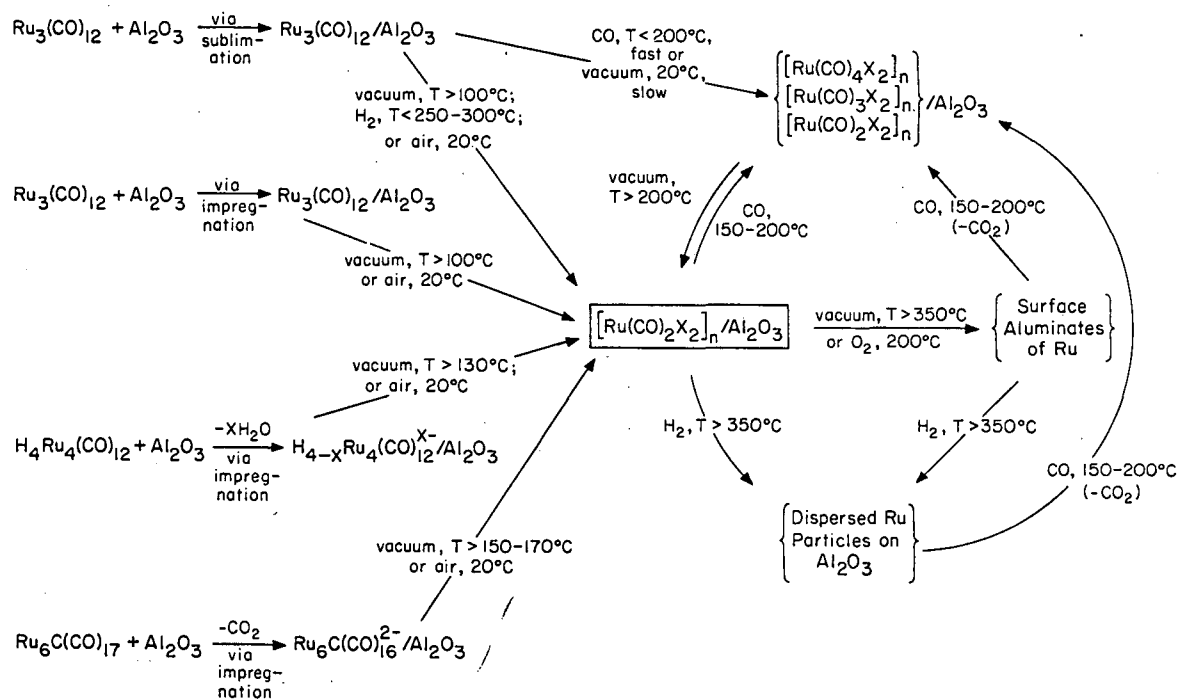


Fig. 1. Relationships between surface structures produced through the decomposition of alumina-supported Ru cluster carbonyls.

surface aluminates. The aluminates are not stable, however, and the initial three structures can be regained by heating in CO. Upon reduction of the supported clusters in H₂ at temperatures above 400°C, Ru microcrystallites appear to be formed. These particles are not stable and the Ru is redispersed into smaller units if the sample is heated in CO above 200°C. The relationship of the different structures formed on the alumina support are shown in Fig. 1.

The distribution of hydrocarbons produced during Fischer-Tropsch synthesis over Ru₃/Al₂O₃ and Ru₆/Al₂O₃ catalysts was practically indistinguishable from that achieved using conventionally prepared Ru/Al₂O₃ catalysts. Likewise, the ratio of olefins to paraffins in the products was comparable for all three catalysts.

The primary characteristic that distinguished these catalysts was activity. A comparison of the turnover numbers for methane formation is presented in Table 1. This measure of catalyst activity is observed to decline with increasing ruthenium dispersion. A further correlation is observed with the ratio of CO to H₂ adsorbed. These data suggest that very highly dispersed ruthenium atoms or clusters do not contribute to Fischer-Tropsch synthesis and that it is only the larger clusters or microcrystallites, bearing a more metallic character, which are active. Further evidence supporting this conclusion has been obtained from in situ infrared spectra, which show that CO chemisorbed on the metal particles participates in reaction but that CO chemisorbed on Ru atoms strongly interacting with the support does not react.

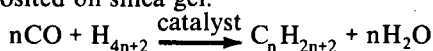
Table 1. Effect of Ru Dispersion on Methane Activity.
Reaction conditions: T = 225°C; P = 10 atm; H₂/CO = 3.

Catalyst	H/Ru	CO/Ru	CO/H	^N CH ₄ (s ⁻¹)
1.3% Ru ₃ /Al ₂ O ₃	0.92	1.94	2.10	1.26 × 10 ⁻³
1.0% Ru ₆ /Al ₂ O ₃	1.18	2.00	1.69	1.67 × 10 ⁻³
3.0% Ru/Al ₂ O ₃	0.54	0.81	1.50	7.13 × 10 ⁻³
11.1% Ru/Al ₂ O ₃	0.30	0.31	1.03	11.98 × 10 ⁻³

HOMOGENEOUS CATALYSTS IN THE REDUCTION OF CARBON MONOXIDE TO HYDROCARBONS

K. Peter C. Vollhardt

Synthesis gas, a mixture of carbon monoxide and hydrogen produced by the controlled combustion of coal in the presence of water, may be converted to hydrocarbons in the presence of an appropriate heterogeneous catalyst. This reaction is called the Fischer-Tropsch reaction, and one of the original catalysts used in this process was cobalt deposited on silica gel.



In this laboratory we have embarked on a program aimed at developing new catalysts for the, we hope, selective reduction of carbon monoxide to defined organic products, for example methane, methanol, or certain hydrocarbon fractions. Particularly strong efforts are directed at the discovery of homogeneous catalytic systems that might allow the elucidation of mechanisms, and that have the potential

for systematic catalyst modification ("catalyst tailoring").

In research carried out along these lines it has been found that a 3% crosslinked, macroporous polystyrene supported cobalt carbonyl complex is catalytically active in Fischer-Tropsch synthesis. The unique aspect of this catalyst is that it is not physically absorbed on the polystyrene matrix but is in fact chemically bound through a η^5 -cyclopentadienyl ligand. In a static reactor, at a starting pressure of hydrogen and carbon monoxide of 75 psig in a 3:1 ratio, and with the catalyst suspended in octane solvent, heating to about 150°C produces methane (84%), higher hydrocarbons (16%), and water. A typical gas chromatographic trace of the octane solubles after several turnovers is shown in Fig. 1.

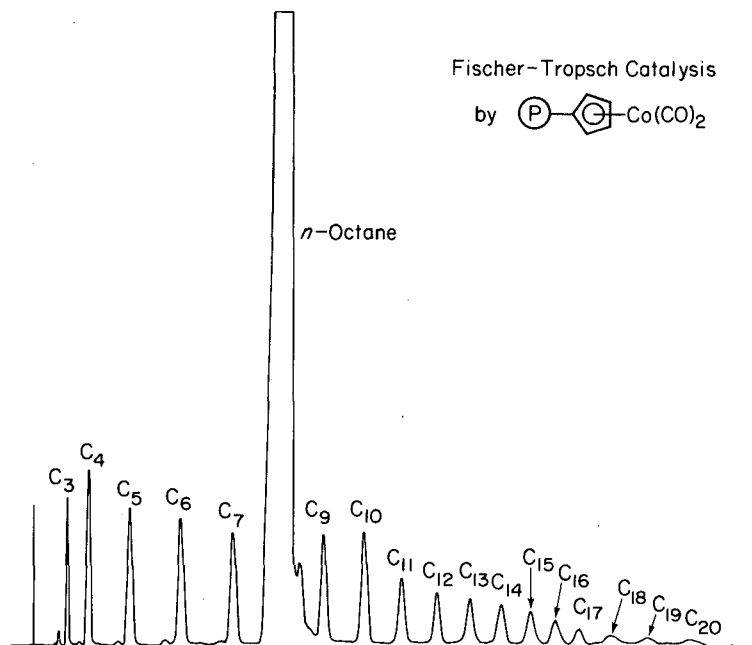


Fig. 1.

The catalyst may be recycled several times with unchanged activity. Controlled experiments show that the catalyst remains associated with the polystyrene resin and that the resin is not degraded during the catalytic cycle. Best activity is achieved when the catalyst is pretreated with heat or light to completely remove the bound carbon monoxide. The original cobalt carbonyl species may, however, be completely regenerated after several catalytic turnovers by pressurization with carbon monoxide. Interestingly, the corresponding unsupported soluble cobalt carbonyl species is not active in the reduction of carbon monoxide but decomposes under the same conditions. When the above Fischer-Tropsch catalysis is carried out with deuterium instead of hydrogen gas, deuterated hydrocarbons are produced, and infrared spectroscopic analysis of the resin shows the incorporation of deuterium into the backbone of the catalyst. This indicates that the polystyrene acts as a unique ligand to the catalytically active species which is capable of hydrogen-deuterium exchange. At high H_2/CO ratios methane is formed almost exclusively at the expense of higher hydrocarbons. The polystyrene-supported catalyst is also unusually selective in the synthesis of normal alkanes, and branched alkanes are being produced in only very small quantities. Analysis of the yields of the individual higher hydrocarbons shows a fit to the Schulz-Flory equation with a chain growth probability factor of 0.83, well in line with the behavior of other Fischer-Tropsch

catalysts. It thus appears that the higher hydrocarbons are formed by a polymerization type mechanism.

The attachment of soluble, homogeneous catalysts to polymer supports has been the subject of considerable recent research activity. Depending on bead and pore size, catalyst distribution, number and structure of pores, concentration and kind of attached ligands, degree of crosslinking, swelling properties of the polymer, and solvent, one may observe changes in rate and product distribution in catalytic processes effected by these catalysts when compared with their mobile counterparts. The polystyrene supported cobalt catalyst mentioned above is the first catalyst activated to new activity on polymer attachment and the first immobilized homogeneous Fischer-Tropsch catalyst. The reproducibility of the results, product distribution, regenerability of catalyst, and the control experiments strongly argue against cobalt crystallites or heterogeneous clusters as being responsible for catalytic action. Since Fischer-Tropsch activity of polymer supported catalysts in solvent suspension has hitherto never been demonstrated, this finding could prove technologically useful in attempts to cope with the problem of heat transfer in this appreciably exothermic process. Experiments aimed at catalyst improvement, elucidation of mechanistic details, and the synthesis of homogeneous, soluble analogs mimicking the polystyrene supported system are the subject of current intensive research.

CARBON MONOXIDE HYDROGENATION OVER CLEAN AND OXIDIZED RHODIUM SINGLE CRYSTALS

Gabor A. Somorjai

The conversion of coal to synthetic fuel has become a problem of major importance in the United States because of (a) the rising cost of crude oil and (b) the abundance of coal in this country. One route involves the gasification of coal in three steps. First a mixture of H_2 and CO is produced by the reaction of water vapor with hot coal ($C + H_2O = CO + H_2$). Then the mixture is enriched in H_2 by the reaction ($CO + H_2O = CO_2 + H_2$). Finally the $CO-H_2$ mixture is reacted over a suitable catalytic surface to produce a mixture of hydrocarbons. On certain catalyst surfaces, nickel for example, only methane (CH_4) forms under appropriate experimental conditions. On other catalyst surfaces (cobalt, iron, rhodium, and thorium oxide for example) a mixture of longer-chain hydrocarbons is produced. This latter process is called the Fischer-Tropsch reaction and was used in

Germany during World War II with a cobalt catalyst to produce low-octane synthetic fuels.

If we are to produce high-quality synthetic fuels, it is essential to understand the mechanism of this reaction on the molecular level. By controlling the catalytic surface structure and composition, one, or only a few, desired product molecules are synthesized. This objective is pursued through physical characterization of the catalyst, identification of the structure and quantity of adsorbed species, and measurements of the reaction kinetics as a function of the surface composition and surface structure.

The reactions of CO and H_2 are commonly divided into two classes: those leading to methane formation (or perhaps methanol) and those that yield molecules in which there are several carbon-carbon bonds (longer chain

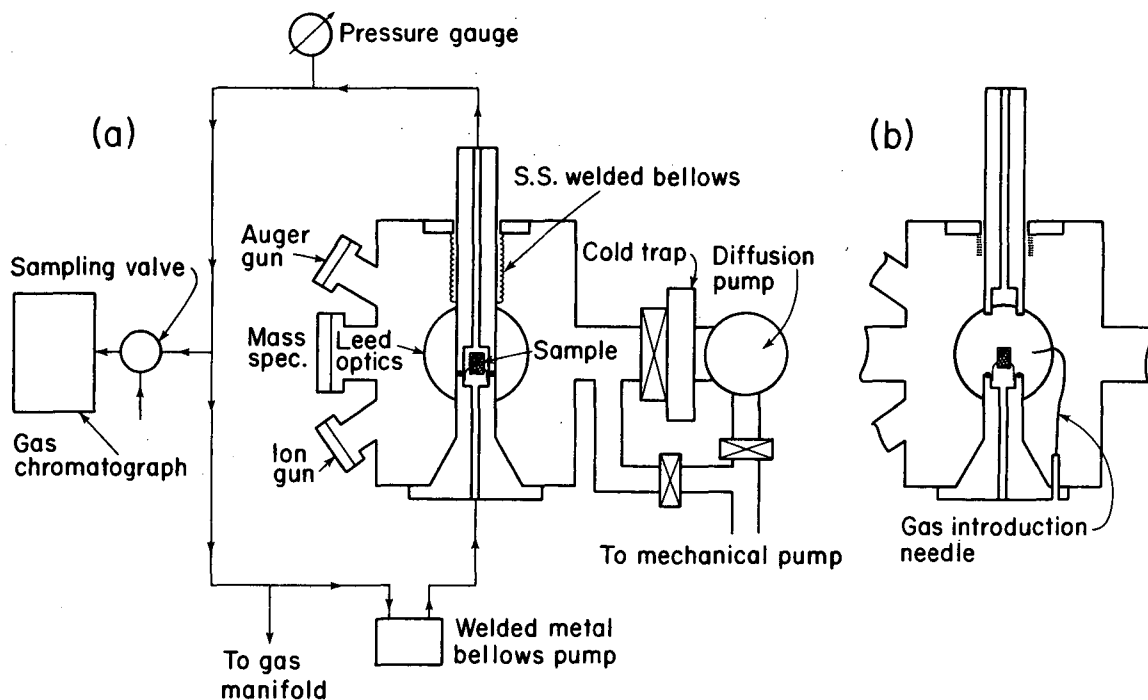


Fig. 1. Scheme of the high pressure apparatus for catalytic reaction studies on crystal surfaces.

hydrocarbons). The latter requires the "insertion" of several carbon species into the molecular chain in addition to hydrogenation, while the former involves only hydrogenation. The rates of both classes of reactions are slow and are controlled by specific surface bond-breaking and bond-forming processes in all conditions of the experiment.

We have studied the formation of hydrocarbons on rhodium crystal surfaces by using a high-pressure low-pressure apparatus that operates in the 10^{-8} Torr to 100 atm pressure range (Fig. 1). The apparatus incorporates many surface analysis features (LEED, AES,

mass spectrometry) and permits analysis of the catalyst surface before and after the high pressure reaction without removing the sample from the reaction chamber. Initially clean rhodium catalysts primarily produced methane at an initial rate of 0.15 molecules/site/second at 300°C and did not produce detectable amounts of oxygenated hydrocarbons. Preoxidation of the rhodium resulted in drastically increased initial reaction rates and the formation of methanol, ethanol, and acetaldehyde. These results suggest that a higher oxidation state of rhodium is needed to produce oxygen-containing hydrocarbons.

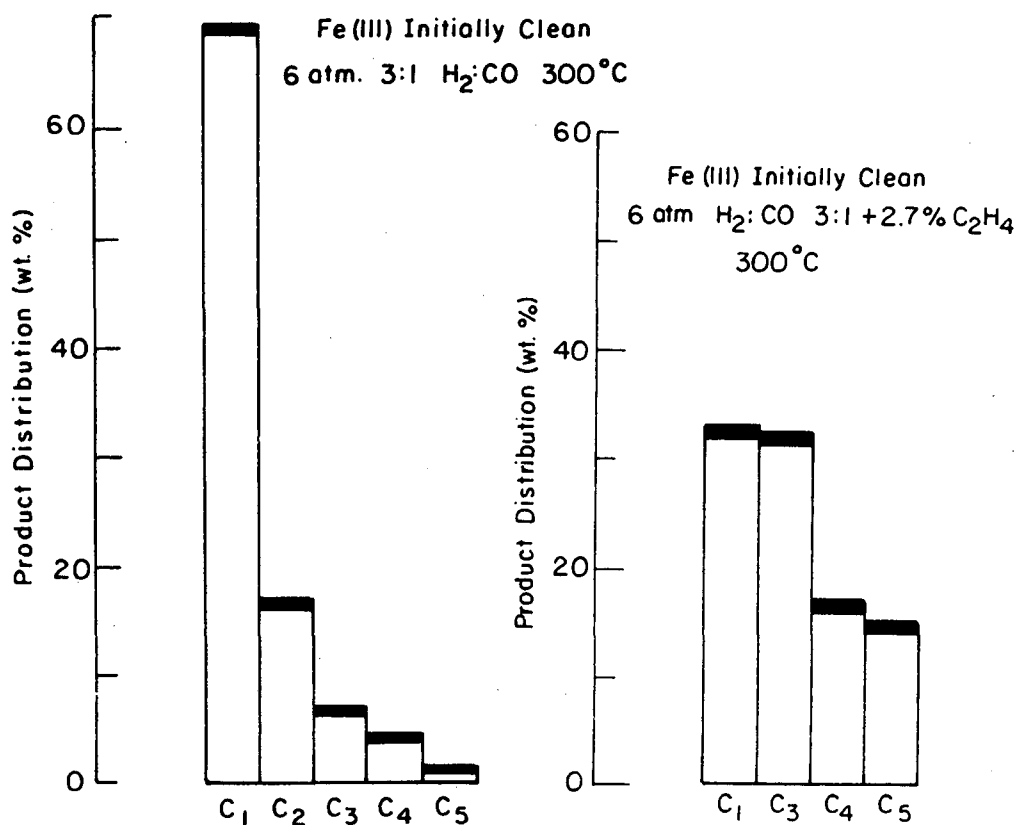


Fig. 2. Comparison of product distribution obtained over Fe(III) with and without C_2H_4 in the reactant gas mixture.

PHOTOCHEMISTRY AT SEMICONDUCTOR SURFACES

Gabor A. Somorjai

Photoexcitation of semiconductor surfaces followed by transfer of the excitation energy to small molecules is one of the most promising means of converting solar energy to chemical fuels. We are studying the reaction chemistry and surface properties of several photoactive oxide semiconductors in an attempt to better understand the factors essential to the efficient promotion of thermodynamically uphill reactions that may be catalyzed by photoexcited semiconductor surfaces.

We have found that hydrogen is generated when a strontium titanate (SrTiO_3) single crystal is illuminated with bandgap (ultraviolet) radiation ($h\nu \geq 3.2$ eV) while immersed in an aqueous alkaline electrolyte or while covered with a water vapor saturated crust of NaOH. Rates of hydrogen production of about 50 monolayers per hour (5×10^{16} molecules/hr cm^2) are obtained using the output of a 500 W high pressure mercury lamp. This rate can be sustained for days, and the amount of hydrogen produced exceeds by far the production expected from a stoichiometric surface reaction. The hydrogen is evolved from the illuminated surface; both electrically insulating stoichiometric crystals and electrically conducting pre-reduced crystals are effective catalysts. Both oxidizing and reducing active sites appear to be photogenerated on the same surface. Therefore, it appears likely that one could carry out a wide

range of redox reactions at both the semiconductor-liquid and semiconductor-gas interfaces.

Coating the back surface of pre-reduced crystals by platinum increases the rate of hydrogen production up to 4500 monolayers per hour. The hydrogen is evolved from the platinum surfaces in this circumstance in analogy to the operation of photoelectrochemical cells.

The rate of hydrogen evolution increases with the hydroxide concentration of the electrolyte. Hydroxide appears to play a role in trapping photogenerated holes and preventing electron-hole recombination. We are studying the role of hydroxides and the nature of surface sites active in the photodissociation of water with a variety of surface analytical techniques.

Photoelectron spectroscopies (UPS and XPS) have identified the presence of hydroxide groups and a reduced Ti^{3+} species on SrTiO_3 (111) surfaces prepared in ultrahigh vacuum. Oxygen binds only to surfaces rich in Ti^{3+} which is oxidized to Ti^{4+} upon the oxygen adsorption. Illumination of the surface with bandgap photons ($h\nu \geq 3.2$ eV) desorbs oxygen and regenerates the Ti^{3+} species. Programmed thermal desorption studies in conjunction with the photoemission work are unravelling the relationship between surface hydroxylation and photoactivity.

COORDINATION CHEMISTRY OF Ni AND Pt METAL SURFACES

E. L. Muetterties

A definition is sought of the structural features and the chemistry of molecules or molecular fragments chemisorbed on nickel and platinum metal crystals as a function of surface crystallography and surface contamination by elements such as carbon. Electron diffraction and spectroscopic techniques in conjunction with chemical studies are used to define structure and chemistry. For example, the chemisorption of benzene on low index surfaces of nickel has been shown definitively to be associative at temperatures below 100°C by the quantitative displacement of C_6D_6 from the surface by trimethylphosphine. Carbon-hydrogen bond breaking processes for Ni(111)- C_6H_6 are relatively fast at ~ 115°C as shown by displacement and H-D exchange in the reaction

of $P(CH_3)_3$ with Ni(111)- C_6D_6 that had been heated to 115°C.

A remarkable effect of carbon on the chemistry of Ni(111) has been shown for CH_3NC where a quantitative and qualitative change in chemistry ensues with carbon build-up on the nickel crystal face. The chemisorption of CH_3NC on the clean surface is irreversible; only hydrogen, and later nitrogen, is evolved on temperature increase. However, on Ni(111) with low carbon coverages of 0.05 to 0.30, the isocyanide is isomerized to CH_3CN which is then desorbed from the crystal face at 90°C. Double labelled studies with CD_3NC and $CH_3N^{13}C$ established the isomerization process to be *intramolecular*.

MECHANISM OF THE REACTION BETWEEN ORGANOTRANSITION METAL ALKYL AND HYDRIDES: A MODEL FOR THE ALDEHYDE-FORMING STEP IN THE OXO PROCESS

Robert G. Bergman

The hydroformylation reaction (oxo process) is one of the oldest and largest applications of homogeneous catalysis in industry. The simplest example of this process is the conversion of ethylene to formaldehyde; two other major commercial uses are the synthesis of butyraldehyde from propylene, and the manufacture of fatty alcohols from higher olefins. These alcohols find application in the production of lubricants, plasticizers and detergents.

Although several of the mechanistic steps in the oxo process are understood mechanistically, one that is not concerns the mode by which metal acyls (which have been established as intermediates in the process) are converted into aldehydes in the last step. The two prime contenders for the mechanism of this step involve (a) oxidative addition of H_2 to the metal, followed by reductive elimination of aldehyde, and (b) bimolecular reaction of a metal hydride with the metal acyl.

Because of the sensitivity of the cobalt and rhodium species utilized as catalysts in the oxo process, it has been difficult to resolve this question in the oxo system itself. As an alternative approach, we have investigated this problem in a related molybdenum system. We have now found that molybdenum hydrides and

alkyls produce aldehyde under very mild conditions. This has provided strong evidence for mechanism (b) summarized above. In addition, our work has helped to understand how this process operates, and identify the M-R plus M-H reaction as a potentially very general transformation in organotransition metal chemistry. Finally, we have found that this type of reaction may also be used to convert alkenes to ketones.

The specific system involves the alkyls and hydride of η^5 -cyclopentadienyl-(tricarbonyl)-molybdenum. As shown in Fig. 1, η^5 -cyclopentadienyl(hydrido)tricarbonylmolybdenum (1) reacts with η^5 -cyclopentadienyltricarbonylmethyl- and ethylmolybdenum (2a and 2b), leading to quantitative yields of acetaldehyde and propionaldehyde, respectively. Reaction with the corresponding benzyl complex (2c) leads to both toluene and phenylacetaldehyde, the ratio of products depending upon the hydride concentration. Crossover experiments have been carried out utilizing η^5 -cyclopentadienyl and η^5 -methylcyclopentadienyl complexes, with one of the pair labeled with deuterium. These demonstrate that the mechanism of this reaction cannot involve metal-carbon bond homolysis leading to alkyl or acyl

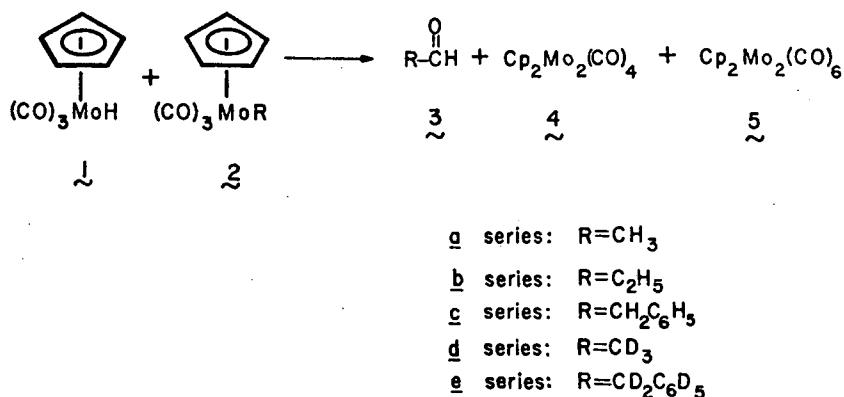


Fig. 1. Reaction between η^5 -cyclopentadienyl(tricarbonyl)hydridomolybdenum and η^5 -cyclopentadienyl(tricarbonyl)alkylmolybdenum complexes.

radicals, except as a minor pathway in the benzyl case. An alternative mechanism involving initial rearrangement of 2 to an acyl complex, followed by entry of hydride 1 into the unsaturated molybdenum coordination sphere and reductive elimination, is postulated.

It has also been found, contrary to an earlier report, that hydride 1 reacts with ethylene to give 3-pentanone and ethane. 3-pentanone is

also formed from 2b and ethylene; similarly, reaction of 2a with ethylene gives 2-butanone. It is postulated that these ketone-forming processes intervene when the molybdenum acyl intermediates are trapped by ethylene rather than hydride. Insertion into the metal-acyl bond, followed by rapid reaction with hydride, then leads to ketonic products (see Fig. 2).

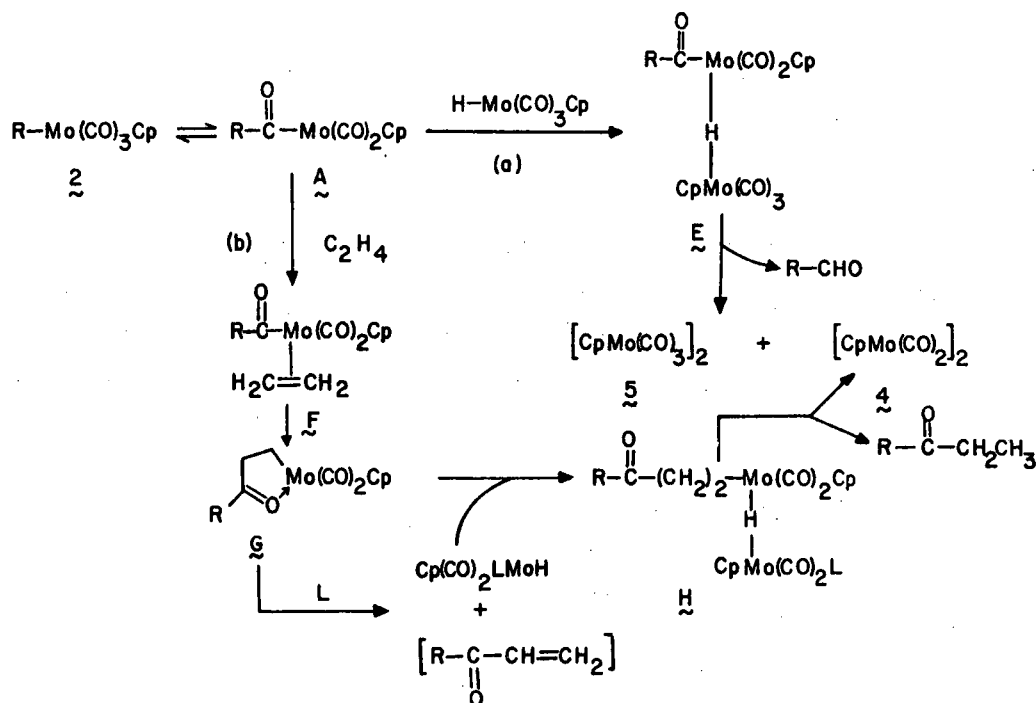


Fig. 2. Postulated mechanism for the reaction between cyclopentadienylmolybdenum hydride and -alkyls, and for the reaction of these molybdenum alkyls with ethylene.

CATALYTIC CRACKING OF n-HEXADECANE

Heinz Heinemann

A brief study was undertaken to determine the effect of liquid water on the rate and product distribution obtained in the catalytic cracking of n-hexadecane over silica-alumina type catalysts. The hypothesis that an increase in Bronstedt acid sites might enhance cracking was not supported. In fact, the rate of cracking was lower in the presence than in the absence of water. Two interesting observations were made: (1) Cracking occurred, though at very low conversions, at temperatures as low as 250°C. This has not been observed previously, probably due to lack of analytical tools to identify very small amounts of products. (2) While all of

four catalysts tested gave more conversion in the absence of water and while conversion was, as expected, a function of acid strength of the catalyst, one catalyst (Catalyst A: 75% silica, 25% alumina) gave a very different product distribution in the presence of water. All other catalysts in the presence or absence of water (and the catalyst A in the absence of water) showed product paraffin/olefin and straight chain/branched chain ratios consistent with a carbonium ion mechanism. Catalyst A in the presence of water gave product characteristics indicative of free radical cracking. This phenomenon has not yet been explained.

THE BUILDING OF NEW CATALYSTS: THE STRUCTURES AND CHEMICAL ACTIVITIES OF ORDERED METAL MONOLAYERS DEPOSITED ON CRYSTAL SURFACES OF OTHER METALS

Gabor A. Somorjai

We are attempting to build catalysts of desired chemical activity and selectivity. This is carried out by depositing ordered layers of metals on single crystal surfaces of other metals. We aim to independently control the atomic structure and composition of the metal monolayers. First a suitable substrate is chosen

that is a metal single crystal with the desired surface structure (geometry, controlled concentrations of step and kink atoms). Then a certain amount of the other metal is deposited in the range of a fraction of a monolayer to several layers on this substrate under appropriate conditions. This is shown in Fig. 1.

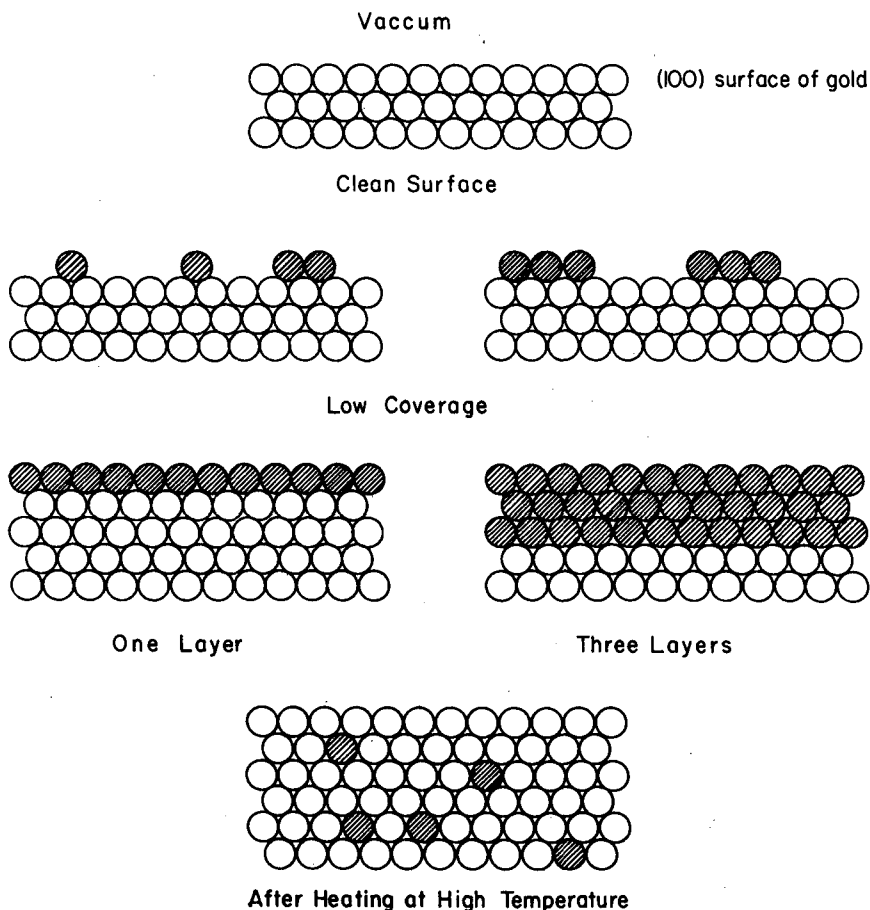
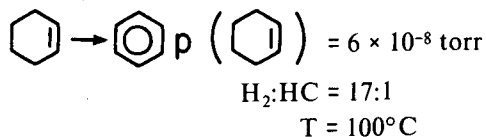


Fig. 1.

At present the Pt-Au and the Ni-K systems are under investigation. In the case of the Pt-Au system platinum deposited on the Au(100) crystal surface, and gold deposited on the Pt(100) crystal surface have been studied. The catalytic activity has been tested with the following reaction:



The results for platinum deposited on the Au(100) crystal surface are shown in Fig. 2. Initially the reaction rate increases linearly with platinum coverage until a plateau is reached at about 1.5 monolayers. This plateau value of the reaction rate, caused by 1.5 or more epitaxially deposited platinum layers is about 6 times higher than that of a platinum single crystal surface with the same atomic surface structure.

The deposition of about one monolayer of gold on Pt(100) also increases the reaction rate, this time by a factor of about 4 over that of the clean Pt(100) crystal surface. This is shown in Fig. 3. The nonzero reaction rate at high gold coverages is due to the crystal edges that do not get covered with gold during deposition.

The absorbed metal atoms can have a number of effects. They can

- block certain chemically active substrate sites,
- create new sites, which are either typical for the adsorbate metal or arise from a unique adsorbate-substrate atomic configuration, and
- accept electrons from or donate electrons to the substrate metal.

These effects play important roles in catalysis and they may influence different surface reactions differently. In this way tailoring the chemical properties of the catalyst is achieved.

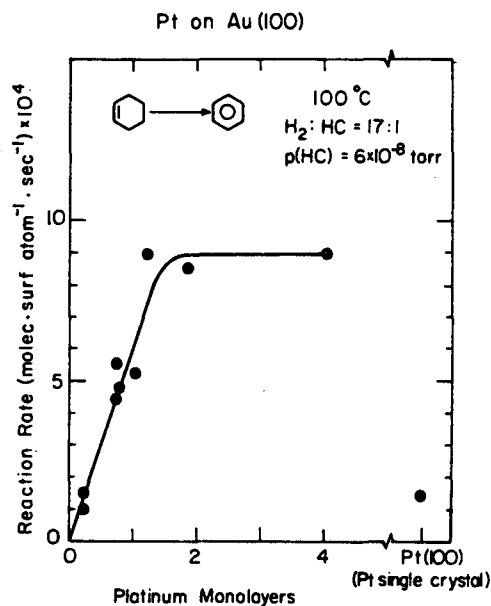


Fig. 2.

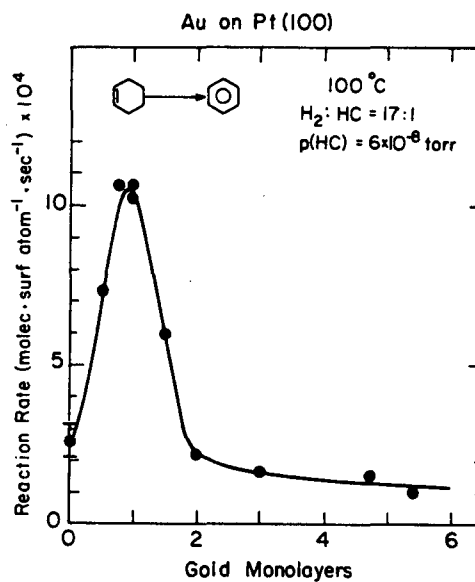


Fig. 3.

HETEROJUNCTIONS

Marvin L. Cohen

Many electronic devices are based on semiconductor-semiconductor interfaces (heterojunctions) e.g., solar cells and solid state lasers. The properties of these interfaces can be quite different from the individual bulk materials. By properly choosing the two materials, the electronic properties of the interface can be tailored for a particular use. However, before such an ideal can be realized, a systematic way of understanding interface properties must be achieved. An attempt at such an understanding has been made in our group.

The lack of periodicity in a heterojunction has made theoretical calculations difficult, but by using the supercell technique in conjunction with self-consistent pseudopotential methods, we are able to calculate the electronic band structure of an interface to an accuracy of ~ 0.1 eV. In addition, we can obtain the *total* self-consistent valence charge densities of *individual* electron states which are important for locating interface states. Interface states are those in which the charge is localized near the interface and are important in determining the transport properties of the junction. We are trying to understand the conditions under which interface states will exist. Calculations have been done on a few prototype heterojunctions: GaAs/AlAs(110), Ge/GaAs(110), Ge/ZnSe(110), GaAs/ZnSe(110), ZnS/ZnS(111-

0001), and ZnSe/ZnSe(111-0001) interfaces. A qualitative conclusion is reached that either ionicity or symmetry change alone can induce interface states. However, the existence of specific interface states is sensitive to the details of the projected band structure. For example, Ge/GaAs and GaAs/ZnSe have similar ionicity difference, but interface states exist in the fundamental gap of Ge/GaAs and not GaAs/ZnSe because the discontinuity in the valence-band maximum is only ~ 0.4 eV for Ge/GaAs while it is 2.0 eV in GaAs/ZnSe.

Recently, a new type of structure called superlattice, which is a series of heterojunctions, has received vast theoretical and experimental interest. Experiments on the GaSb-InAs superlattice system have shown that such a system can undergo a transition from semiconductor to semimetal by varying the thickness of the superlattice cell. Our supercell technique is directly applicable to the superlattice geometry. Calculations on the GaSb-InAs system were performed. A direct theoretical confirmation on the semiconductor-semimetal transition cannot be obtained because the size of the supercell needed for the transition exceeds our computing limits. However, many interesting effects due to the superlattice geometry still can be learned from these calculations.

ELECTRONIC STRUCTURES AT SCHOTTKY BARRIERS

Marvin L. Cohen

Metal-semiconductor interfaces (Schottky barriers) have been studied extensively because of their interesting behavior and their importance in device technology. Experimentally, two qualitatively different characteristics of the Schottky barriers are observed depending on the semiconductors involved. For covalent semiconductors like Si or Ge, the barrier height, Φ_b , is found to be essentially independent of the metal contact; i.e., the Fermi level is pinned. For ionic materials like SiO_2 , the barrier height increases almost linearly with the electronegativity, χ_m , of the metal in contact. This linear dependence is measured by the interface index $S \equiv \Phi_b / \gamma \chi_m$.

To understand this behavior, the electronic structures of various Schottky barriers are studied theoretically using the self-consistent pseudopotential method. Pseudopotentials, representing the effective interaction between the core and the valence electrons, are derived

to fit the atomic properties of individual elements. For given crystal structures, valence electrons are allowed to distribute themselves self-consistently. Because of computational limitations, the metal is simulated by a jellium model for the positive background with an average charge density of aluminum.

Si, GaAs and Ge have been studied for covalent materials. In all cases, a high density of metal-induced states are found in the forbidden gap which is responsible for the Fermi-level pinning. These states are free-electron-like in the metal and decay exponentially into the semiconductor. The exponential tail provides available states on the semiconductor side (otherwise, electronic states are forbidden), and they give rise to Fermi-level pinning. Similar calculations for diamond, ZnSe and ZnS Schottky barriers indicate that these states are less and less available until finally S becomes close to 1 for very ionic materials such as ZnS.

PLASMA ENHANCED DEPOSITION OF MAGNETIC THIN FILMS

Dennis W. Hess

A continuing aspiration of surface science and particularly of thin film technology involves the attainment of specific surface and bulk properties of materials by deliberate variation of surface preparation or deposition methods. Current synthetic methods for thin film fabrication are quite inflexible due to the small number of deposition variables available. However, the use of a glow discharge (plasma) to promote chemical reactions makes available numerous parameters which can be used to "build properties into" inorganic film materials during deposition.

Thin films ($\sim 1 \mu\text{m}$) of iron/iron oxide are being deposited by striking a glow discharge in iron pentacarbonyl vapor. As expected, the crystallinity of the deposits, as measured by x-ray diffraction patterns, is a strong function of substrate temperature, and displays an amorphous film character until a critical temperature ($\sim 200^\circ\text{C}$) is reached. At this temperature, a diffraction peak corresponding to $\alpha\text{-Fe}$ is observed. This critical temperature can be varied somewhat by a change in power level. Further, the diffraction peak decreases as the power level increases. These results indicate that the relative amount of amorphous iron (or

iron as Fe_2O_3 or FeO_4) in the film is increasing with power, and this trend is probably a result of increased ion and/or electron bombardment as well as enhanced incorporation of carbon and oxygen (as indicated by chemical analyses) due to the plasma-enhanced decomposition of carbonyl groups.

The magnetic properties of the plasma deposited films are being investigated with a hysteresigraph. The films do not display magnetic properties at temperatures below 150°C . However, above 150°C , the hysteresis loop is a strong function of substrate temperature and rf power. The ratio of the remnant induction to the saturation induction increases with increasing temperature and increasing power. Similarly, the coercive force increases with substrate temperature and rf power level. Since an increase in coercive force often results from structural imperfections and inhomogeneities, it appears that an increase in power increases the number of structural defects. This result correlates well with the observed loss of crystallinity discussed above. Additional plasma parameters will be studied to determine the limits of magnetic film properties attainable with plasma enhanced deposition.

GRAIN BOUNDARIES AND IONIC CONDUCTION IN SODIUM BETA ALUMINA

L. C. De Jonghe

Sodium beta aluminas exhibit an unusually high ionic conductivity and a negligible electronic conductivity, making them useful as solid electrolytes. Such solid electrolytes are the important elements of high energy density sodium/sulfur storage batteries. Sodium conduction in the hexagonal beta alumina crystals takes place exclusively along the basal planes; the ionic conduction anisotropy is approximately 10^{15} at 300°C . During dc ionic conduction in polycrystalline solid electrolytes, the sodium ions must be transported through grain boundaries. Due to the crystal structure anisotropy, one may suspect that the ionic resistivity for intergranular transport will depend significantly on the details of the grain boundary structure. The anisotropy of the crystal structure and of the conductivity permits us to

consider two extreme cases. On the one end of the grain boundary resistivity scale, one can consider completely blocking grain boundaries as shown in Fig. 1. This lattice image shows a grain boundary containing a (00.1) faceted grain boundary. The lattice fringes are the 00.2 fringes and can be thought of as representing the conduction planes. Sodium transport through such grain boundaries is structurally impossible. At the other end of the grain boundary resistivity scale, one can consider low angle grain boundaries with various habit planes. Low angle grain boundaries can be frequently found in sintered beta aluminas. These simple tilt boundaries are made up of dislocations with a Burger's vector of $\frac{1}{2}C_0$. This corresponds exactly to the spacing of the conduction planes in the beta alumina crystal structure. An

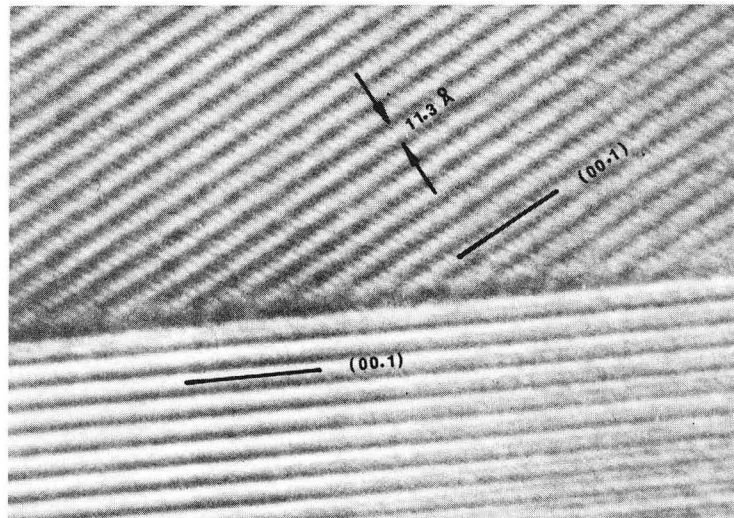


Fig. 1. Lattice image of a 00.1 faceted blocking grain boundary.

example of such a grain boundary is shown in Fig. 2. It is an asymmetrical tilt boundary, the structure of which can be interpreted in terms of a much simplified model. This simplified model has been found to be useful for sodium beta alumina grain boundaries since the transmission electron microscope observations clearly indicated that the grain boundary structure is such that the conduction planes attempt to match across it.

When impurities such as calcium are present, blocking intergranular layers may be formed.

An example of such a blocking intergranular layer is shown in Fig. 3. The intergranular phase is calcium hexaaluminate. When solid electrolytes of the beta alumina family contain calcium, the ionic resistivity is strongly affected, as shown in Fig. 4. The effect of impurities on the resistivity and the lifetime of a solid electrolyte in a battery will be investigated further. This is an important area of research, since the lifetime of the solid electrolyte determines the cost of the energy storage system.

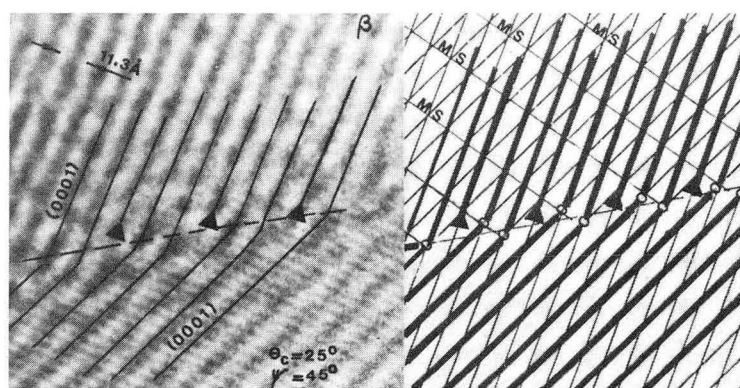


Fig. 2. Asymmetrical tilt boundary; (a) lattice image (11.3 Å); (b) corresponding geometry of the simplified model.

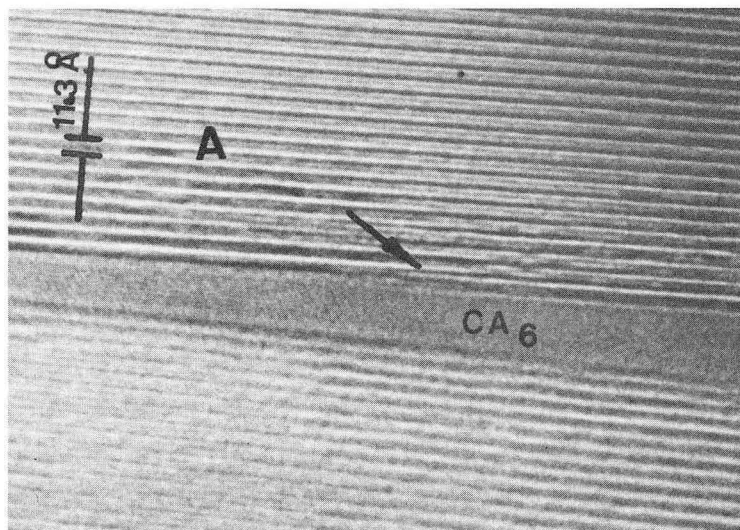
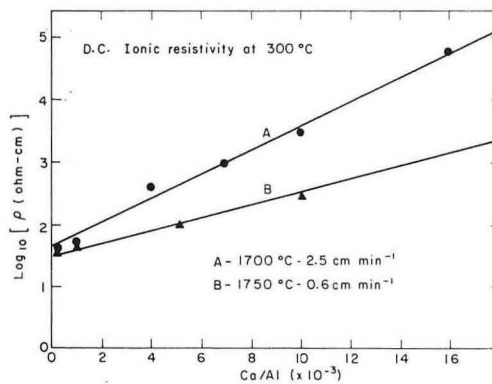


Fig. 3. Detail of an intergranular region containing calcium hexa-aluminate (CA_6). In the beta alumina grain marked A, a single spinel edge on an 00.1 faceted interface is indicated by an arrow. Calcium/aluminum - 0.03; sample rapidly sintered at $1700^\circ C$.

Fig. 4. Specific dc ionic resistivities at 300°C for samples sintered under different conditions. (A) 1700°C; (B) 1750°C. The results show that the dependence of the ionic resistivity on calcium content is semi-logarithmic, and depends on the sintering conditions.



GRAIN BOUNDARY PHASES IN SILICON NITRIDE CERAMICS

Gareth Thomas

Silicon nitride is the leading contender for the high strength, high temperature material to be used in gas turbines operating at temperatures some 300°C higher than now. It is oxidation and corrosion resistant, has a high strength/weight ratio, excellent thermal shock resistance and unsurpassed intrinsic high temperature mechanical properties. Its development into a fully useful material has however been hampered by the difficulty of manufacturing a 100% dense polycrystalline Si_3N_4 solid. The usual hot-pressing and liquid-phase sintering techniques use additives with properties much inferior to Si_3N_4 , and it has been suggested that these form thin amorphous films at most grain boundaries, with very unfavorable effects on the high temperature properties.

Figure 1(a) is a bright field (BF) image showing the microstructure of commercial hot-pressed Si_3N_4 (NC 132), but the magnification is insufficient to show if grain boundary amorphous films exist. Lattice imaging can probe the grain boundary structure at a resolution necessary to detect the ultrathin amorphous films, but it can analyze only a small boundary segment at a time. With dark field (DF) imaging [Fig. 1(b)], relatively large areas of the sample can be examined in just one micrograph. The objective aper-

ture is placed over a diffuse diffraction ring due to the amorphous phase, while matrix Bragg reflections are carefully excluded. (When this is not possible, recording images at two or more different specimen tilts will distinguish the crystalline phases from the amorphous ones.) The bright parts of the DF image are then due to the amorphous phase. The fact that all the grain boundaries in Fig. 1(b) appear bright shows that this phase wets them all. Quantitative results on the boundary phase width can be obtained by taking a microdensitometer trace across a boundary and comparing the total area under the peak with the image intensity of a larger pocket of amorphous material in a nearby specimen area. In this way the width of the glassy phase at several of the boundaries (e.g., between points A-A' and B-B' on the figure) was determined to be $15 \pm 5 \text{ \AA}$.

To minimize the adverse effects of the thin amorphous film, it is important to control its composition so that impurities which lower its softening temperature are excluded. We have examined the composition of all the constituent phases in a number of silicon nitrides by detecting the element-specific x rays generated in a scanning transmission electron microscope. Correlating the results with the mechanical properties above 1000°C

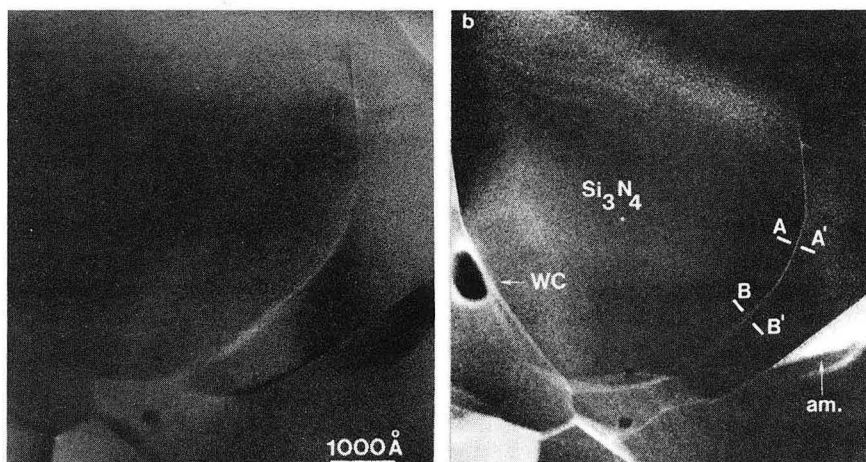


Fig. 1. (a) Bright field and (b) dark field images of silicon nitride. The bright lines at the grain boundaries in (b) show that all boundaries are penetrated by the amorphous phase.

has confirmed that the presence of minute amounts of impurities such as Ca will significantly lower the material's strength. Figure 2 illustrates this point with a pair of x-ray spectra taken from a material with particularly poor high temperature properties. Although the total concentration of Ca in the whole sample (spectrum a) is less than 0.3% in the amorphous phase, the concentration is 4% (spectrum b). At this concentration Ca lowers the melting point of the amorphous phase to below

1400°C thus making the whole material totally unusable.

Figure 3 shows a BF-DF pair from a material closely related to Si_3N_4 , Be Sialon, prepared by hot-pressing with no additives. The absence of a bright line at the grain boundary shows that there is no glassy phase. This material is therefore expected to retain its rigidity to much higher temperatures. It indicates that way toward future improvements in these important materials.

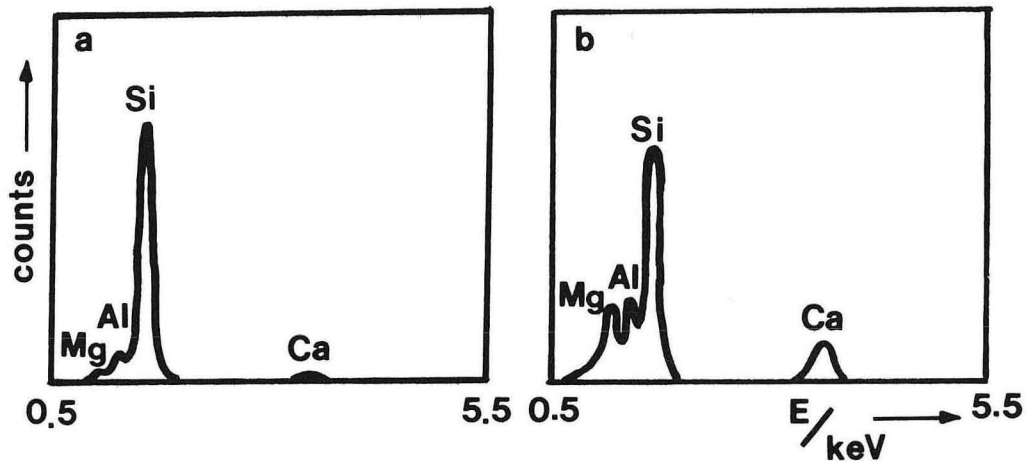


Fig. 2. X-ray spectra from (a) a large region of MgO-fluxed silicon nitride and (b) the amorphous phase. Notice that Ca concentration is much higher in (b) than (a).

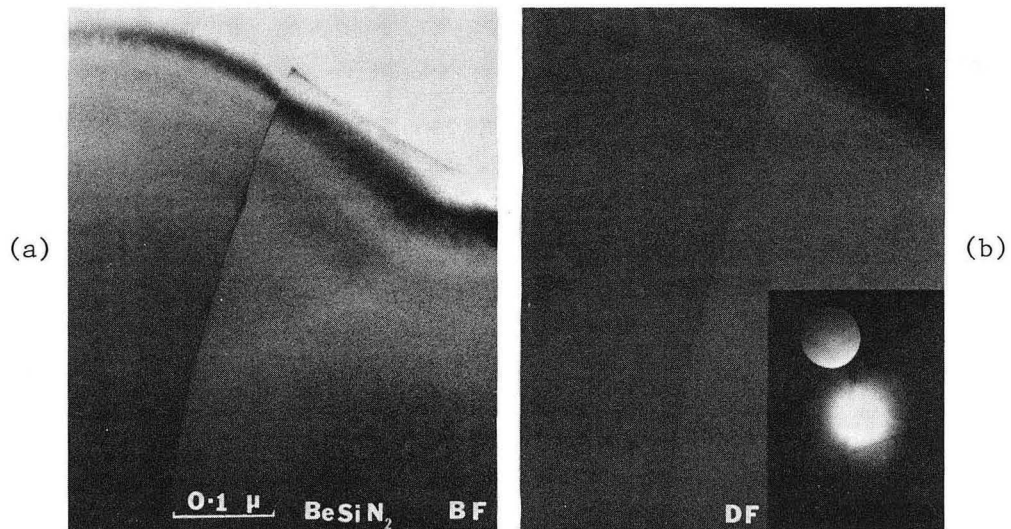


Fig. 3. (a) Bright field and (b) dark field in a hot-pressed BeSi_3N_4 . The absence of a bright line at the grain boundary in (b) shows that there is no intergranular amorphous phase.

INTERFACES IN DUPLEX FERRITE MARTENSITE (DFM) STEELS

Gareth Thomas

DFM steel is a two-phase alloy containing a controlled amount of a strong second phase (martensite) in a ductile matrix (ferrite) to develop the desired combination of strength and formability. The martensite constituent carries the major portion of the applied load, and the matrix provides the essential element of ductility.

A successful new series of high strength, formable Fe/2%Si/0.1%C steels heat treated to form duplex ferrite martensite structure have been developed, which provide a potential candidate for energy saving applications (e.g., automobiles). This alloy was patented by the Department of Energy (U.S. Patent #4,067,756).

The mechanical behavior of the DFM alloy is primarily controlled by the principle of fiber strengthening, and thus as in many other composite materials the nature of the strong second phase/matrix interfaces plays an important role in determining mechanical properties. That is, strong particles that do not have good atomic fit with the matrix are known to act as sites for failure by decohesion or to encourage the formation of interfacial micro-cracks at the weak interface between

particles and matrix. Therefore a good bond is necessary to prevent interface failure and to enable the full toughness of the ferrite to be realized.

Figure 1(a) shows the duplex microstructure in fibrous morphology developed in the Fe/2%Si/0.1%C steel. The high resolution microscopy was successfully applied to reveal the detailed atomic arrangement across the α /martensite interface [Fig. 1(b)]. As the (110) fringes cross the interface, they are distorted but are continuous except for occasional end-on dislocations. Such high degree of coherency is essential for effective load transfer, and should be in part the origin of the superior ductility at high strength levels of this structure. The lattice imaging technique not only provides the striking information on the characterization of the interface at atomic level but also enables the measurement of carbon contents in the martensite constituent, which is another critical factor influencing toughness properties. In this way, the coherency at the interface and carbon concentration are properly controlled so as to achieve optimum mechanical properties of the duplex steels.

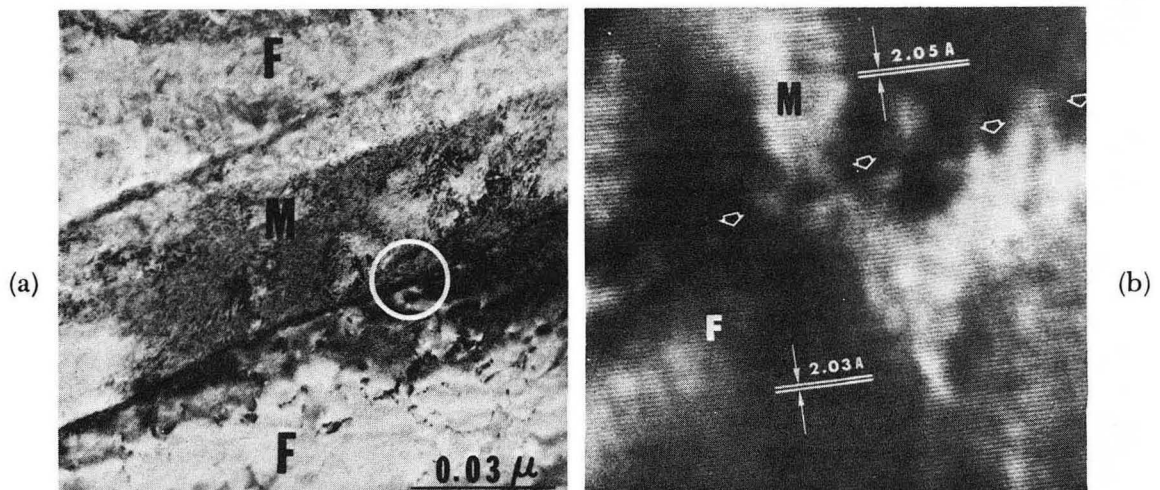


Fig. 1. Conventional bright field (a) and lattice image (b) of an α /martensite interface in the 2% Si DFM steel. The lattice image (b) was taken from the area encircled in (a). Martensite tetragonality creates the larger d_{101} spacing in the martensite region (M), with respect to the ferrite (F). The arrows indicate the interface.

AUSTENITE/MARTENSITE INTERFACES IN HIGH STRENGTH TOUGH STRUCTURAL STEELS

Gareth Thomas

Martensite transformation in structural steels is characterized by numerous interfaces such as twin, lath, packet, grain boundaries, and interphase interfaces such as carbide/martensite or austenite/martensite. These interfaces either by themselves or due to secondary processes such as segregation and/or precipitation can in a significant way influence the deformation and fracture behavior of high strength martensitic structural steels. Therefore, an important aspect of structural alloy design is the detailed characterization of these interfaces at the highest available resolutions.

It is shown that the microduplex struc-

ture consisting of strong phase lath martensite (major phase) and ductile interlath retained austenite (minor phase) offers by far the best combinations of high strength and excellent toughness. Since the mechanical properties of such a microduplex structure would be highly sensitive to the lath martensite/retained austenite interface characteristics, high resolution lattice imaging of this interface is performed and an example of this is shown in Fig. 1. Three different fringes can be seen: (i) the $(110)_M$ fringes extending on either side of the austenite phase, (ii) the $(111)_A$ austenite fringes, and (iii) the larger d-spacing Moiré fringes at the interface.

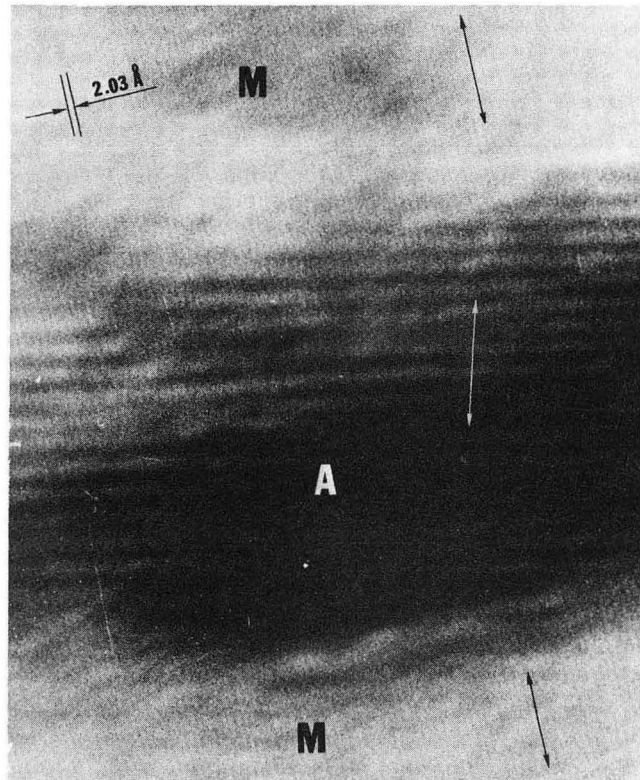


Fig. 1. Lattice image micrograph at austenite (A)/martensite (M) interface in a medium C structural steel.

Considerable bending of the $(110)_M$ martensite fringes and the high degree of coherence at the interface can be seen. Initial real space measurements indicate significant C enrichment in austenite. The presence of Moiré fringes indicate that the interface is not exactly edge-on. In addition, they also reveal the presence of ledges at the austenite/martensite interface, confirming an earlier model proposed to explain the wide scatter in the habit plane measurements of lath martensitic transformation. This model,

schematically illustrated in Fig. 2, clearly shows that—depending on ledge morphology and density—a macroscopic habit plane can be either different from [Fig. 2(b)] or the same as [2(c)] the microscopic habit plane. Thus, in addition to providing valuable information on interface characteristics, lattice imaging is also extremely useful in gaining a fundamental understanding of the nature and mechanism of various transformations (in this case, ledge mechanisms of growth).

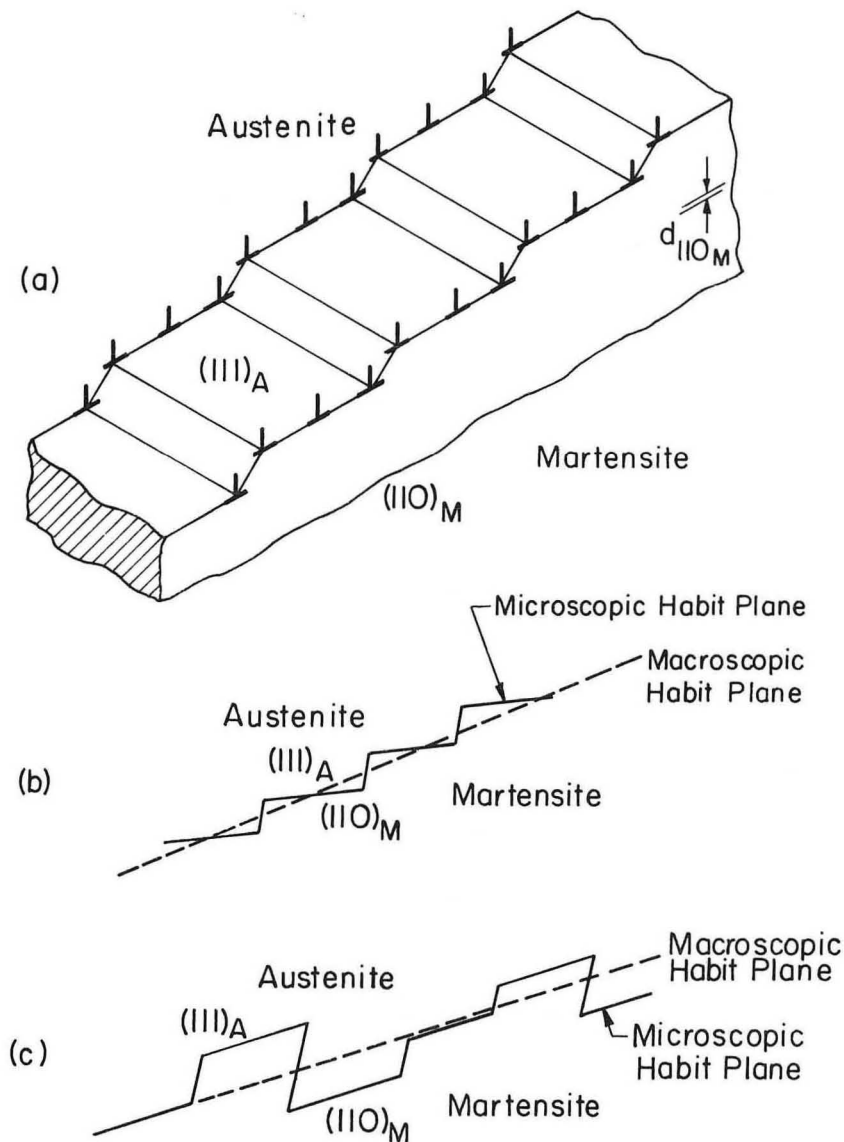


Fig. 2. (a) Suggested ledge model of the austenite/martensite interface. (b) and (c) Different ledge configuration leading to either different macroscopic and microscopic habit planes (b) or a single habit plane (c).

ATOMIC STRUCTURE OF GRAIN BOUNDARIES IN SEMICONDUCTORS

Gareth Thomas

While LEED and other surface analytical techniques have opened up the study of atomic arrangements on solid surfaces, the atomic structure of *internal* surfaces and defects such as grain boundaries has remained relatively unknown. With the advent of high resolution electron microscopes with point-to-point resolution of 2.5 Å or better, the atomic structure of bulk defects can now be studied directly. The power of the newly available technique is illustrated very vividly in a study of a Ge grain boundary carried out on a prototype electron microscope in Japan [O. L. Krivanek, S. Isoda, and K. Kobayashi, *Phil. Mag.* 36, 931-940 (1977)].

The boundary was of the 39° tilt type and was observed end-on along [011] direction at 500 kV under essentially kinematical conditions. An enlarged image of the boundary is shown in Fig. 1. The white dots correspond to empty channels running through the crystal along the [011] direction, which are bounded by six-fold rings of Ge atoms.

At the boundary 15 white dots are larger than the rest. These dots were inter-

preted as arising from larger channels, and a model in which they correspond to channels of seven-fold rings was built. The model shows excellent agreement with the original image [Fig. 2(a) model, (b) experiment, (c) simulation].

The details of the structure can be seen in Fig. 3. The tilt boundary consists of alternating rings of five-fold and seven-fold rings, each pair of rings accommodating a 1/2 [011] edge dislocation. There are no dangling bonds—the bonding requirements of each Ge atom are perfectly satisfied.

Figure 4 shows two possible core configurations for the [011] edge dislocation in a diamond-cubic lattice derived by Hornstra in 1958 but never experimentally verified. Comparison with Fig. 3 shows that in the 39° tilt boundary, only type b occurs. This finding is very important in the quest for detailed understanding of structural, mechanical, and electrical properties of grain boundaries and other internal surfaces.

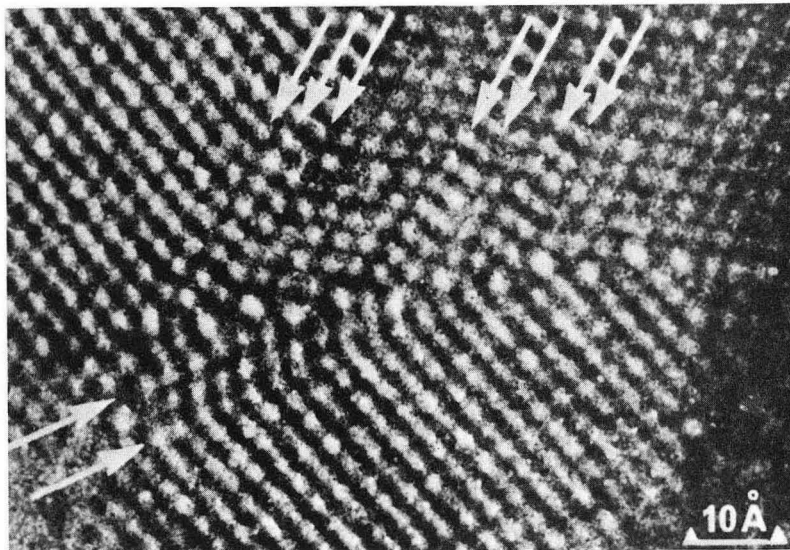


Fig. 1. An electron image of a grain boundary in Ge.

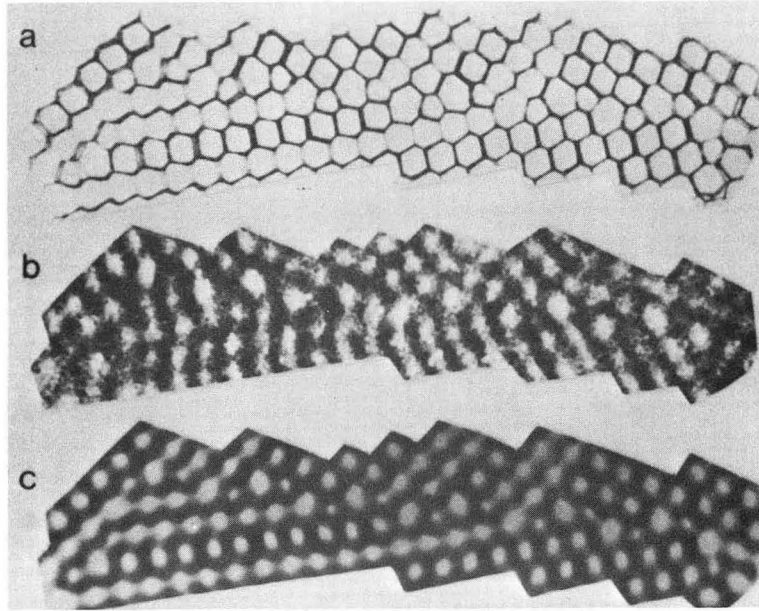


Fig. 2. Model for the grain boundary (a) deduced from the image (b) gives an excellent simulation of the image (c).

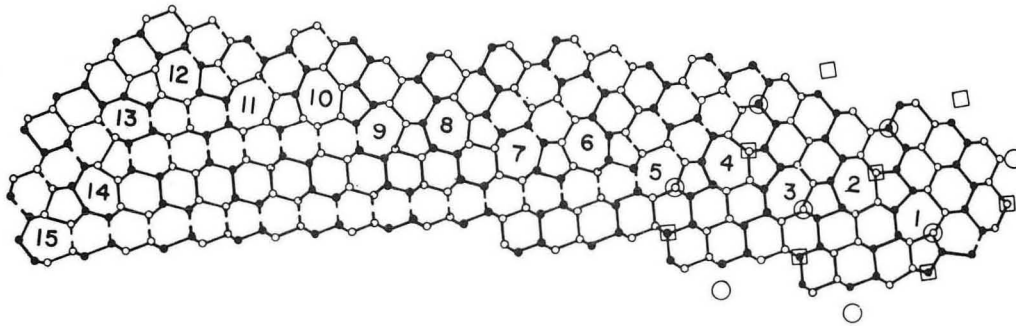


Fig. 3. Details of the model. The seven-membered rings at the boundary are numbered.

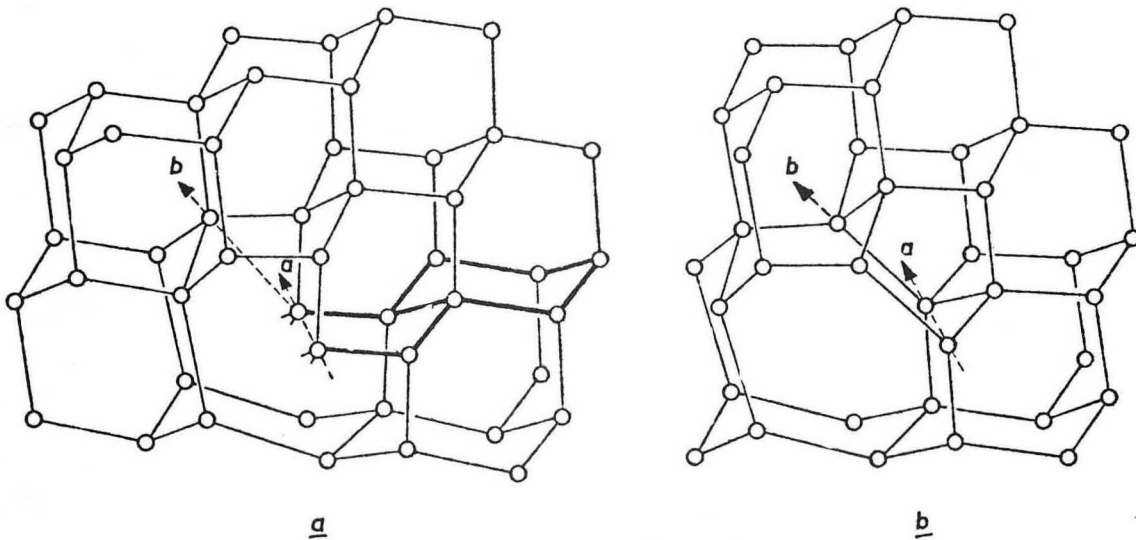


Fig. 4. Two models for the edge dislocation in Ge. Only type (b) has been observed in this study.

STRUCTURE OF THE Si - SiO₂ INTERFACE

Gareth Thomas

The Si - SiO₂ interface is technologically one of the most important interfaces in all of modern industry. It is the basic working element of the metal-oxide-semiconductor field-effect-transistor (MOSFET), which constitutes one of the basic elements of the integrated electronic circuit. Its structure has been probed by a variety of techniques such as ion backscattering, Auger spectroscopy, XPS and ESCA, all used in conjunction with ion-beam profiling. The results on the whole have been rather inconclusive, mainly because of the very poor spatial (x-y) resolution of these analytical techniques (~ 1000 Å at best) as well as the poor depth resolution (~ 20 Å).

By preparing a thin (100-200 Å thick) cross section of the interface and viewing it edge-on along the [011] direction, the structure of the interface can be studied at about 3 Å resolution by high resolution electron microscopy (O. L. Krivanek et al., in Proceedings of the International Conference on the Physics of SiO₂ and Its Interfaces, IBM, 1978). Figure 1 shows 900 Å long segments of three different interfaces. The straight lines serve as reference markers; the arrows denote "hills" on the Si surface. The transition from the silicon crystal

into the oxide is seen to be quite abrupt and the interfaces remarkably straight, except for modulations of $\sim 4-8$ Å height and a wavelength of 200-500 Å.

Higher magnification images in which the Si crystal lattice is directly resolved (Fig. 2) show that the transition from the silicon into the amorphous oxide occurs within ≤ 3 Å, contrary to some earlier claims. They also reveal one-plane-high atomic steps on the crystal surface, separated by 20-40 Å. These are 3.2 Å high on the (111) interface, but only 1.4 Å (d₄₀₀) on the (100) interface, a distance too small to be resolved by present-day microscopes in the axial mode, but resolvable in the tilted illumination mode (bottom image).

Surface steps cause scattering of the electron gas that flows on the silicon side of the interface in a working MOSFET. This effect is especially important at high gate voltages, which compress the two-dimensional gas against the interface. The values for surface roughness derived from the magnitude of the scattering effect show excellent agreement with our direct results. This provides much encouragement for our future work correlating the electrical properties with the atomic structure of materials.

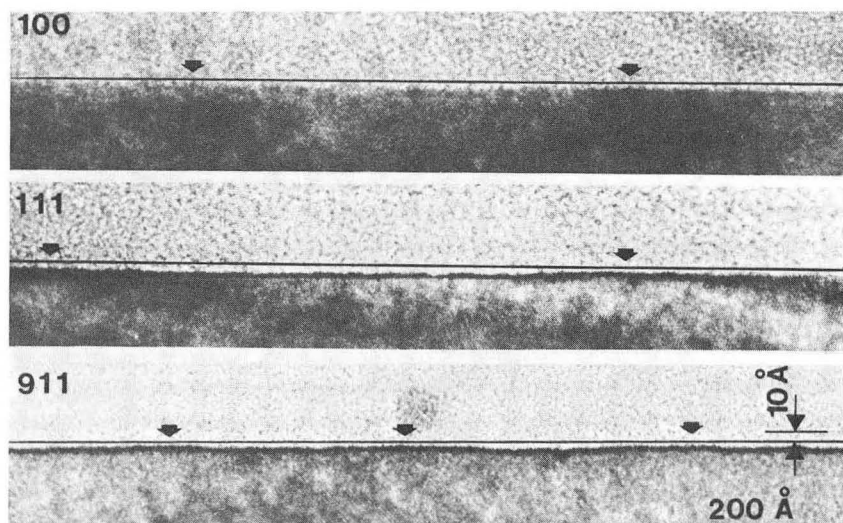


Fig. 1. Images of three types of Si-SiO₂ interface [(100), (111) and (911)]. The arrows mark "hills" on the Si crystal.

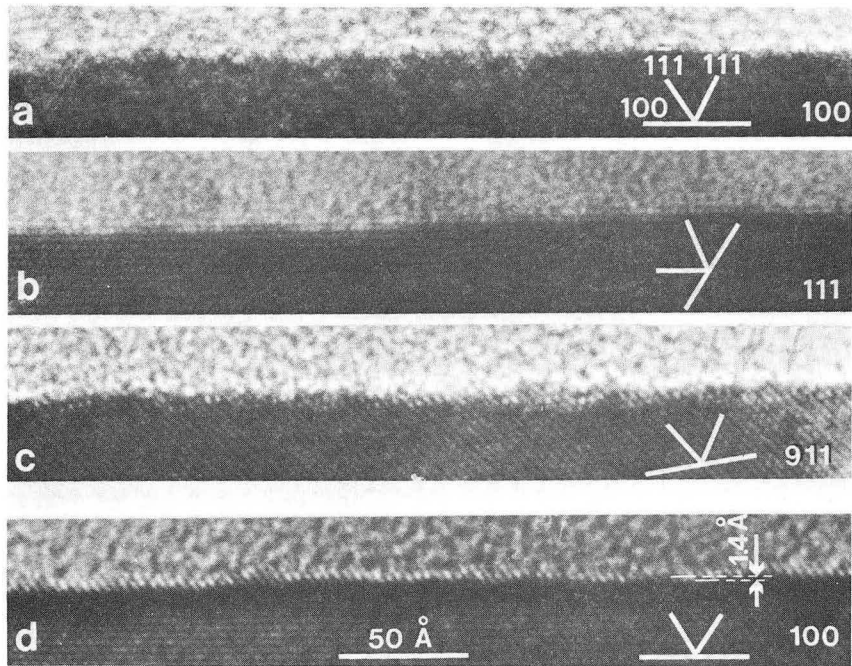


Fig. 2. High-magnification views of the interfaces. (111) and (200) lattice planes are directly resolved.

RESEARCH STAFF

The research staff consists of students (undergraduate and graduate), postdoctoral fellows and staff members at LBL, and faculty members in various departments at the Berkeley campus of the University of California.

Students:

S. L. Abensohn	M. -D. Huang
S. G. Avanzino	J. Ihm
A. J. Baca	N. S. Jacobson
J. A. Baker	A. H. Janowicz
J. J. Barton	S. M. Johnson
M. A. Berg	C. S. Kellner
C. Berman	S. D. Kevan
C. S. Blair	L. E. Klebanoff
H. E. Bryndza	R. J. Koestner
W. J. Cannella	P. K. Lam
R. G. Carr	H. S. Lee
M. Chang	T. H. Lin
J. Chao	G. G. Low
S. L. Chiang	H. S. Luftman
S. S. Chiang	S. Marks
P. B. Comita	W. McKee
P. Cornelius	D. P. Mobley
J. Crowell	J. E. Northrup
T. T. Dai	R. Osório de Cerqueria
S. M. Davis	C. C. Parks
R. F. Davis	M. I. Perez
R. A. Dictor	P. Perkins
D. F. Dooley	T. A. Reis
L. H. Dubois	H. J. Robota
J. G. Ekerdt	S. Roche
J. D. Ewing	D. H. Rosenblatt
M. R. K. Farnaam	K. Sakai
P. L. Flaitz	S. Salim
T. J. Fredrick	K. Shanahan
C. Friend	T. M. Shaw
B. Fultz	S. A. Sherrow
R. J. Gale	D. Stern
S. Gandhi	N. D. Taylor
E. Garfunkel	J. D. Tersoff
S. George	J. G. Tobin
W. D. Gillespie	M. -C. Tsai
J. H. Goble, Jr.	M. K. Vernon
G. Goncher	F. T. Wagner
W. L. Guthrie	M. Wax
B. C. Hale	D. Wexler
A. Harris	P. M. Whitmore
R. F. Hicks	L. M. Williams
P. Hislop	M. Yin
W. E. Hollingsworth	D. A. Zwemer
D. V. Horak	

Postdoctoral fellows and staff members

N. T. Allison
H. Arakawa
H. Auweter
M. Balooch
L. S. Benner
D. T. Beruto
A. Campion
R. G. Carr
K. M. Chang
U. Dahmen
P. Davies
D. J. Dwyer
S. Ferrer
J. E. Frommer
J. Frost
A. Gin
J. M. Huggins
Z. Hussain
T. Iri
B. Joós
J. -Y. Koo

O. L. Krivanek
M. Langell
T. -H. D. Lee
J. A. Little
W. -J. Lo
T. P. Lockhart
A. J. Machiels
M. A. Maier
D. J. Meschi
R. K. Mishra
J. A. Roberts, Jr.
J. W. A. Sachtler
H. Schmid
F. Schwager
C. K. Syn
A. Tomsia
K. Urabe
M. A. van Hove
P. R. Watson
D. Westerman
Y. Zundeleovich

Faculty and Principal Investigators:

Alexis T. Bell, Department of Chemical Engineering
Robert G. Bergman, Department of Chemistry
Marvin L. Cohen, Department of Physics
Lutgard C. DeJonghe, Department of Materials Science and Mineral Engineering
James W. Evans, Department of Materials Science and Mineral Engineering
Leopoldo M. Falicov, Department of Physics
Ronald Gronsky, Department of Materials Science and Mineral Engineering
Charles B. Harris, Department of Chemistry
Heinz Heinemann, Department of Chemical Engineering
Dennis W. Hess, Department of Chemical Engineering
William L. Jolly, Department of Chemistry
Yuan T. Lee, Department of Chemistry
Alan V. Levy, Molecular and Materials Research Division, LBL
John W. Morris, Department of Materials Science and Mineral Engineering

Earl L. Muetterties, Department of Chemistry
Rolf H. Muller, Department of Chemical Engineering
Donald R. Olander, Department of Nuclear Engineering
Joseph A. Pask, Department of Materials Science and Mineral Engineering
Paul A. Richards, Department of Physics
Philip N. Ross, Molecular and Materials Research Division, LBL
Alan W. Searcy, Department of Materials Science and Mineral Engineering
David A. Shirley, Department of Chemistry
Gabor A. Somorjai, Department of Chemistry
Gareth Thomas, Department of Materials Science and Mineral Engineering
Peter C. Vollhardt, Department of Chemistry
Kenneth H. Westmacott, Molecular and Materials Research Division, LBL
David P. Whittle, Department of Materials Science and Mineral Engineering
John S. Winn, Department of Chemistry

LEGAL NOTICE

This book was prepared as an account of work sponsored by an agency of the United States Government. Neither the United States Government nor any agency thereof, nor any of their employees, makes any warranty, express or implied, or assumes any legal liability or responsibility for the accuracy, completeness, or usefulness of any information, apparatus, product, or process disclosed, or represents that its use would not infringe privately owned rights. Reference herein to any specific commercial product, process, or service by trade name, trademark, manufacturer, or otherwise, does not necessarily constitute or imply its endorsement, recommendation, or favoring by the United States Government or any agency thereof. The views and opinions of authors expressed herein do not necessarily state or reflect those of the United States Government or any agency thereof.

This report was done with support from the Department of Energy. Any conclusions or opinions expressed in this report represent solely those of the author(s) and not necessarily those of The Regents of the University of California, the Lawrence Berkeley Laboratory or the Department of Energy.

Reference to a company or product name does not imply approval or recommendation of the product by the University of California or the U.S. Department of Energy to the exclusion of others that may be suitable.

This work was supported by the Division of Materials Sciences and Chemical Sciences, Office of Basic Energy Sciences, U. S. Department of Energy